UC Santa Cruz

UC Santa Cruz Previously Published Works

Title

A genetically encoded fluorescent acetylcholine indicator for in vitro and in vivo studies.

Permalink

https://escholarship.org/uc/item/6cc7v9pp

Journal

Nature biotechnology, 36(8)

ISSN

1087-0156

Authors

Jing, Miao

Jing, Miao

Zhang, Peng

et al.

Publication Date

2018-09-01

DOI

10.1038/nbt.4184

Peer reviewed

eScholarship.org Powered by the California Digital Library
University of California

Author Manuscript

Author Manuscript

Author Manuscript

Author Manuscript

HHS Public Access

Author manuscript

Nat Biotechnol. Author manuscript; available in PMC 2019 January 09.

Published in final edited form as:

Nat Biotechnol. 2018 September ; 36(8): 726–737. doi:10.1038/nbt.4184.

ED SUM: Signaling by the neurotransmitter acetylcholine is monitored in cells and animals with a sensitive reporter.:

A genetically encoded fluorescent acetylcholine indicator for *in vitro* and *in vivo* studies

Miao Jing[#1,2,3], **Peng Zhang**[#4], **Guangfu Wang**[4,5], **Jiesi Feng**[1,2,3], **Lukas Mesik**[6], **Jianzhi Zeng**[1,2,3], **Huoqing Jiang**[1,2,3], **Shaohua Wang**[7], **Jess C. Looby**[4,8], **Nick A. Guagliardo**[4], **Linda W. Langma**[9], **Ju Lu**[9], **Yi Zuo**[10], **David A. Talmage**[7], **Lorna W. Role**[7], **Paula Q. Barrett**[4], **Li I. Zhang**[6], **Minmin Luo**[11,12], **Yan Song**[3], **J. Julius Zhu**[4,13,14,15,17], and **Yulong Li**[1,2,3,17]

[1]State Key Laboratory of Membrane Biology, Peking University School of Life Sciences, Beijing 100871, China [2]PKU-IDG/McGovern Institute for Brain Research, Beijing 100871, China [3]Peking-Tsinghua Center for Life Sciences, Beijing 100871, China [4]Department of Pharmacology, University of Virginia School of Medicine, Charlottesville, VA 22908 [5]Center for Life Sciences, School of Life Science and Technology, Harbin Institute of Technology, Harbin 150001, China [6]Zilkha Neurogenetic Institute, Department of Physiology & Neuroscience, Keck School of Medicine, University of Southern California, Los Angeles, CA, 90033 [7]Department of Neurobiology and Behavior, Stony Brook University, Stony Brook, NY 11794 [8]Undergraduate Class of 2019, University of Virginia College of Arts and Sciences, Charlottesville, VA 22908 [9]Department of Surgery, University of Virginia School of Medicine, Charlottesville, VA 22908 [10]Department of Molecular, Cell, and Developmental Biology, University of California, Santa Cruz, CA 95064 [11]School of Life Sciences, Tsinghua University, Beijing 100084, China [12]National Institute of Biological Sciences, Beijing 102206, China [13]School of Medicine, Ningbo University, Ningbo, 315010, China [14]Donders Institute for Brain, Cognition and Behavior, Radboud University Nijmegen, 6525 EN, Nijmegen, Netherlands [15]Department of Physiology, School of Basic Medicine, Tongji Medical College, Huazhong University of Science and Technology, Wuhan 430030, China

[#] These authors contributed equally to this work.

Users may view, print, copy, and download text and data-mine the content in such documents, for the purposes of academic research, subject always to the full Conditions of use:http://www.nature.com/authors/editorial_policies/license.html#terms

[17]Correspondence and requests for materials should be addressed to Julius Zhu (jjzhu@virginia.edu) and Yulong Li (yulongli@pku.edu.cn). Manuscript correspondence: Yulong Li (yulongli@pku.edu.cn).

AUTHOR CONTRIBUTIONS

J.J.Z. and Y.L. conceived the project. M.J. did GACh screening and optimization as well as its validation in cultured neurons and IPN slices. Y.L., Y.S., J.Z. and H.J. designed and performed the work on transgenic flies. M.J. and J.F. preformed experiments related to calcium imaging, GPCR internalization Tango assay and FRET measurements. L.M. and L.I.Z. did *in vivo* imaging of GACh sensors in mouse visual cortex. M.L. supervised the imaging experiments on MHb-IPN brain slices. P.Z. and G.W. together carried out the other experiments with assistance and advice from S.W., J.C.L., N.A.G., L.W.L., J.L., Y.Z., D.A.T., L.W.R., P.Q.B. and J.J.Z. All authors contributed to data analysis. M.J., P.Z., G.W., J.J.Z. and Y.L. wrote the manuscript with input from other authors.

Data availability statement

The plasmid pDisplay-GACh2.0 (#106073) have been deposited to Addgene database (deposit #74965).

Competing interests statement

The authors declare competing financial interests. M.J. and Y.L. have filed patent applications whose value might be affected by this publication.

Author Manuscript Author Manuscript Author Manuscript Author Manuscript

Abstract

The neurotransmitter acetylcholine (ACh) regulates a diverse array of physiological processes throughout the body. Despite its importance, cholinergic transmission in the majority of tissues and organs remains poorly understood owing primarily to the limitations of available ACh-monitoring techniques. We developed a family of G-protein-coupled receptor activation-based ACh (GACh) sensors with sensitivity, specificity, signal-to-noise ratio, kinetics and photostability suitable for monitoring ACh signals *in vitro* and *in vivo*. GACh sensors were validated with transfection, viral and/or transgenic expression in a dozen types of neuronal and non-neuronal cells prepared from multiple animal species. In all preparations, GACh sensors selectively responded to exogenous and/or endogenous ACh with robust fluorescence signals that were captured by epifluorescence, confocal and/or two-photon microscopy. Moreover, analysis of endogenous ACh release revealed firing pattern-dependent release and restricted volume transmission, resolving two long-standing questions about central cholinergic transmission. Thus, GACh sensors provide a user-friendly, broadly applicable tool for monitoring cholinergic transmission underlying diverse biological processes.

INTRODUCTION

Acetylcholine (**ACh**), the first identified neurotransmitter, mediates cell-to-cell communication in the central and peripheral nervous systems, as well as non-neuronal systems[1–7]. Cholinergic projection neurons within the mammalian brain primarily originate in three major nuclei, including the basal forebrain (**BF**), the brainstem pedunculopontine and laterodorsal tegmental nuclei. Cholinergic neurons within these groups project widely throughout the cortical and subcortical domains, consistent with their involvement in complex brain functions, including attention, perception, associative learning and sleep/awake balancing[1–5]. Additional smaller populations of cholinergic neurons scatter throughout other brain areas (e.g., the medial habenula (**MHb**) and the striatum), contributing to behaviors related to motion, motivation and stress[1, 3, 8]. Dysregulation of central cholinergic transmission is linked to a number of brain disorders, including Alzheimer's disease, addiction, epilepsy, Parkinson's disease, schizophrenia and depression[9, 10]. In the peripheral nervous and non-nervous systems, ACh is released by both neurons and non-neuronal cells to relay fast transmission at neuromuscular junctions and to regulate functions of a variety of other tissues and organs, including the heart, liver and pancreas[5–7]. Dysregulation of peripheral and non-neuronal cholinergic signals is associated with multiple pathological states, including cardiovascular disease, diabetes, immune deficiency and cancer[11, 12].

Despite the significance of ACh signals in many fundamental aspects of our physiology, cholinergic transmission in the majority of tissues and organs remains poorly understood, due primarily to the limitations of tools available for the direct measurement of ACh[1, 5, 13]. Microdialysis, an established method for monitoring extracellular ACh[14], is less frequently used because of its poor spatial and temporal resolution. Patch-clamp recordings have excellent sensitivity and temporal resolution, but the approach is limited by the number of cells that can be recorded simultaneously and the prominent desensitization of cholinergic currents[3]. Similarly, ACh amperometry has millisecond temporal resolution, yet its

Author Manuscript Author Manuscript Author Manuscript Author Manuscript

technically challenging enzymatic coating procedure limits its stability and reproducibility[15]. While the TANGO assay has unparalleled sensitivity, the time-consuming transcriptional and translational amplification processes prevent its use for real-time ACh measurements[16]. Recently developed FRET sensors and cell-based fluorescent sensors (CNiFERs) for ACh have attractive real-time imaging features, but they are limited by either the low sensitivity[17, 18] or the dependence on invasive cell transplantation[19, 20]. These fluorescent sensors, nevertheless, inspired us to engineer more user-friendly and broadly applicable genetically-encoded ACh sensors[19, 21].

Here, we report a family of genetically-encoded G-protein-coupled receptor activation-based sensors for ACh (GACh). Our GACh sensors were initially constructed by coupling a circular permutated green fluorescent protein (cpGFP) into a muscarinic acetylcholine receptor (MR), with subsequent improvements via large-scale site-directed mutagenesis and screening. The sensitivity and utility of GACh sensors were validated in cultured HEK293T cells, in cultured cortical neurons, in tissue slices prepared from multiple brain regions and peripheral organs, in the olfactory system of living *Drosophila* and in the visual cortex of awake behaving mice *in vivo*. Our data indicate that GACh sensors have the sensitivity ($EC_{50} \approx 1$ μM), specificity (comparable to endogenous MRs), signal-to-noise ratio (SNR ≈ 14), kinetics ($\tau_{on/off} \approx$ 200–800 ms) and photostability (≥1–4 hrs) suitable for precise and convenient real-time assays of ACh signals.

RESULTS

Development and optimization of GACh sensors

We first inserted a conformationally sensitive cpGFP into the third intracellular loop (ICL_3) of five subtypes of human muscarinic acetylcholine receptors (M_{1-5}Rs) (**Fig. 1a** and **Supplementary Fig. 1**). ICL_3 was chosen because it links the transmembrane helices 5 and 6 of MRs and may undergo a large conformational change upon ACh binding[22]. We replaced ICL_3 of M_{1-5}Rs with a shorter 54-amino acid ICL_3 modified from the structurally well-characterized β_2 adrenergic receptor (β_2AR)[23] to avoid creating a lengthy cpGFP-containing ICL_3 that may hinder the expression and trafficking of the proteins (**Supplementary Fig. 1a**). Cells expressing the M_3R chimera showed excellent membrane expression in HEK293T cells and increased fluorescence responses ($\Delta F/F_0$) (by ~30%) to bath application of ACh (**Fig. 1b** and **Supplementary Fig. 1a**). In contrast, cells expressing the other four MR chimeras all exhibited poor membrane expression and no detectable $\Delta F/F_0$ upon ACh application (**Supplementary Fig. 1b-d**).

To improve this new ACh sensor (named GACh1.0), we used site-directed mutagenesis to create a library of 723 randomized point mutations at the N-terminus two-amino acid and C-terminus five-amino acid linkers that connect cpGFP and M_3R (**Fig. 1c** and **Supplementary Fig. 2; Online Methods**). When expressed in HEK293T cells, we found variants with one or multiple single-point mutations on the seven linker residues (total 18 hits) produced relatively larger $\Delta F/F_0$ responses, with the best variant (named GACh1.5) producing a ~70% increase in $\Delta F/F_0$ (**Fig. 1c,d** and **Supplementary Fig. 2**). In a second round of site-directed mutagenesis and screening, we used combinations of single top hits on N-terminus linker residues (i.e., GG) and 2–4 top hits on C-terminus linker residues, and found one variant

Author Manuscript Author Manuscript Author Manuscript Author Manuscript

(named GACh2.0) out of 23 combinatorial variants with the best $\Delta F/F_0$ (**Fig. 1c** and **Supplementary Fig. 2**). GACh2.0 had the same expression and membrane trafficking properties and enhanced dynamic range (by 2.5-fold) compared to GACh1.0 (**Fig. 1e-g; Supplementary movie 1**), and ~20-fold larger peak signal responses and ~60-fold higher signal-to-noise ratio (**SNR**) compared to M_1R-based FRET sensor[18] (**Fig. 1h-j** and **Supplementary Fig. 3**).

Characterization of GACh sensors in cultured cells

Next, we measured the response kinetics of GACh2.0 (**Fig. 2a,b**). High-speed imaging showed that rapid local perfusion of agonist ACh or antagonist tiotropium (**Tio**) elicited increases or decreases in fluorescence intensity of GACh2.0, with average activation (on) and inactivation (off) time constants of 280 ± 32 ms and 762 ± 75 ms, respectively (**Fig. 2b,c**). These values were likely overestimated due to the slow drug application/perfusion system (~80 ms delay, **Supplementary Fig. 4**). Moreover, confocal imaging indicated that GACh sensors had a photostability comparable to or better than GCaMP6s and EGFP (**Supplementary Fig. 5**). Altering extracellular pH with buffers (pH 5–9) resulted in modest fluorescence changes in GACh expressing cells (**Supplementary Fig. 6a,b**), suggesting a weak pH-dependency. In the permeabilized condition, the fluorescence of GACh sensors exhibit larger pH-dependency with a pKa close to 7 (**Supplementary Fig. 6c,d**).

To measure the sensitivity of GACh2.0, we progressively increased ACh from 10 nM to 100 μM, which increased the fluorescence intensity in GACh2.0 expressing cells, yielding an EC_{50} of ~0.7 μM (**Fig. 2d,e**), a value comparable to wild type M_3Rs[26]. ACh-induced fluorescence signals were completely blocked by co-application of 20 μM AF-DX 384, another muscarinic antagonist[27], indicating specific responses. We also characterized the downstream signaling of GACh sensors. GACh2.0 expressing cells exhibited less receptor internalization in the presence of ACh, as well as reduced TANGO assay signal (β-arrestin-dependent) compared to wild type M_3Rs expressing cells (**Supplementary Fig. 7a,b**). Moreover, the coupling efficiency from GACh2.0 to the Gq-dependent calcium signaling was ~7-fold smaller compared to wild type M_3Rs (**Supplementary Fig. 7c-e**), and there was no detectable coupling between GACh2.0 to the Gs-dependent signaling pathway (**Supplementary Fig. 7f-h**).

We next verified several properties of GACh sensors in cultured rat cortical neurons (**Fig. 2f-j**). Approximately 48 hours after transfection, GACh1.0 and GACh2.0 were expressed throughout the neuronal membrane, with the majority of sensors delivered to the neurites (**Fig. 2f**). ACh enhanced the fluorescence intensity of GACh1.0 and GACh2.0 by ~30% and ~90%, respectively (**Fig. 2g; Supplementary movie 2**), validating their functionality in neurons. Varying ACh concentration in the bath solution from 10 nM to 100 μM progressively increased the fluorescence intensity in GACh2.0 expressing neurons, with an EC_{50} of ~2 μM (**Fig. 2h**). In contrast, bath application of nicotine, choline, glycine, serotonin (5-HT), epinephrine, GABA, glutamate, dopamine, norepinephrine, histamine, and adenosine did not induce any detectable fluorescence responses. Moreover, ACh-induced fluorescence responses were blocked by bath applied Tio (**Fig. 2i,j**). Finally, we noted no alteration in membrane fluorescence intensity in GACh2.0 expressing neurons during a 30-

Author Manuscript Author Manuscript Author Manuscript Author Manuscript

minute bath application of 100 μM ACh (**Supplementary Fig. 8a-c**), consistent with the minimal arrestin-dependent internalization (**Supplementary Fig. 7a,b**).

Validation of GACh sensors in cultured brain slices

To generalize the applicability of GACh sensors, we expressed them in CA1 pyramidal neurons in cultured mouse hippocampal slices. Two-photon imaging showed that GACh1.0, GACh1.5 and GACh2.0 were expressed throughout CA1 pyramidal neurons by lentiviral system, with evident fluorescence signals at the plasma membrane of somata, dendrites and spines, sites of excitatory synapses (**Supplementary Fig. 9**). Next, we chose Sindbis viral expression system that permitted a more rapid (~18 hours) and robust expression of GACh sensors (**Supplementary Figs. 10a and 11a; Online Methods**). Fluorescence responses captured by an epifluorescence microscope showed that a brief 500-ms puff application of ACh or a muscarinic agonist, oxotremorine[26], evoked fluorescence responses in CA1 neurons expressing GACh1.0, GACh1.5 or GACh2.0, whereas puff application of a nicotinic receptor agonist, nicotine, or control bath solution ACSF, induced no responses in same neurons (**Supplementary Figs. 10b-d** and **11b; Supplementary movies 3 and 4**).

Focusing on GACh2.0 that produces the largest $\Delta F/F_0$, we found that repetitive puffs induced the same fluorescence responses in GACh2.0 expressing CA1 neurons (**Supplementary Fig. 12**), indicating robust photostability. As a control, bath application of 1 μM atropine, a muscarinic antagonist[27], but not 2,2,6,6-tetramethylpiperidin-4-yl heptanoate (TMPH), a nicotinic antagonist[28], completely blocked ACh-induced fluorescence responses in GACh2.0 expressing neurons (**Supplementary Fig. 12**). Simultaneous patch-clamp recordings showed that the resting membrane potential, input resistance, membrane time constant and average spiking frequency of GACh2.0 expressing CA1 neurons were not different from nearby control non-expressing neurons (**Supplementary Fig. 13a-d**), suggesting no effect of GACh2.0 expression on basic membrane properties. Moreover, AMPA, NMDA or GABAergic responses, or paired pulse facilitation of AMPA responses in GACh2.0 expressing neurons remained unchanged (**Supplementary Fig. 13e-h**), indicating no alteration of synaptic transmission by GACh2.0 expression. Collectively, these results are consistent with the finding that GACh2.0 is a selective, photostable ACh sensor with minimal perturbation on cellular physiology.

To compare GACh2.0 imaging with patch-clamp recordings, we simultaneously made whole-cell recordings and fluorescence imaging from pairs of neighboring GACh2.0 expressing and non-expressing CA3 pyramidal neurons, which performed robust current response to cholinergic stimulation in cultured mouse hippocampal slices[29](**Fig. 3a**). A 500-ms ACh puff evoked a brief, large inward current followed by a prolonged, small inward current in both GACh2.0 expressing and non-expressing neurons, presumably representing activation of endogenous nicotinic and muscarinic receptors, respectively[3] (**Fig. 3b,d**). A concurrent fluorescence signal was observed only in GACh2.0 expressing neurons, but not in control non-expressing CA3 neurons (**Fig. 3b,c**). The latencies of cholinergic currents and fluorescence responses were the same in GACh2.0 expressing neurons (**Fig. 3b,e**), indicating that GACh2.0 detected ACh as fast as endogenous cholinergic receptors. SNR of GACh2.0 fluorescence responses (~14) seemed to be smaller than that of the fast nicotinic-

Author Manuscript Author Manuscript Author Manuscript Author Manuscript

like cholinergic currents (~35), but larger than that of the slow muscarinic-like cholinergic currents (~8) (**Fig. 3b,f**), indicating a relatively comparable sensitivity for GACh2.0 to electrophysiological recording in monitoring cholinergic signals. The second ACh puff evoked same fluorescence responses, but smaller cholinergic currents (reduced by ~40%) in GACh2.0 expressing neurons compared to the first ACh puff (**Fig. 3b,g,h**), due presumably to the desensitization of endogenous receptors[3]. There was no difference in the amplitude, latency or SNR of cholinergic currents in GACh2.0 expressing and non-expressing neurons (**Fig. 3b-f**), further confirming that expression of GACh2.0 had little non-specific effect on CA3 neurons.

GACh sensors in acute brain slices

We next imaged the fluorescence response of GACh2.0 in acute slices of distinct neuronal preparations, including layer 2 (L2) stellate neurons and L1 interneurons in the medial entorhinal cortex (MEC), L5 pyramidal neurons in the barrel cortex of mice, GABAergic thalamic reticular neurons and glutamatergic thalamocortical neurons in the ventral basal nucleus of rats. Approximately 18 hours after *in vivo* Sindbis viral expression and acute slice preparation, we measured $\Delta F/F_0$ responses to a brief puff application of ACh (**Supplementary Fig. 14a**). ACh and oxotremorine, but not nicotine or control bath solution ACSF, evoked robust fluorescence increases in GACh2.0 expressing neurons in all the preparations (**Supplementary Fig. 14**).

To further test whether GACh2.0 can report endogenously released ACh, we measured $\Delta F/F_0$ responses of GACh2.0 expressing entorhinal L2 stellate neurons to electrical stimulation of MEC L1 (**Fig. 4a**), a layer that is densely innervated by cholinergic fibers originating from BF[30, 31]. In GACh2.0 expressing neurons, twenty pulses at 2-Hz evoked robust fluorescence responses in GACh2.0 expressing neurons (**Fig. 4b; Supplementary movie 5**), and repeated electrical stimuli delivered every 8 minutes induced the same $\Delta F/F_0$ responses in GACh2.0 expressing neurons (**Fig. 4c,d**), indicating the suitability of GACh2.0 in monitoring ACh signals over long periods. Systematically varying the stimulation frequency revealed that low frequency stimuli (0.5−2 Hz) evoked large, plateau-like fluorescence responses, intermediate frequency stimuli (4−12 Hz) elicited more rapidly rising but briefer fluorescence responses, while high frequency stimuli (≥32 Hz) induced minor fluorescence responses (**Fig. 4e-g**). Given that BF cholinergic neurons in behaving animals prefer low frequency (~0.5−2 Hz) tonic firing and theta rhythmic (~4−12 Hz) phasic firing[32,33], these results suggest that these two preferred firing patterns generate distinct sustained or transient ACh release. Further altering the number of electrical pulses delivered at 2-Hz showed that single pulses elicited detectable $\Delta F/F_0$ responses, whereas multiple pulses induced enhanced $\Delta F/F_0$ responses (**Fig. 4h-j**), suggesting the possible scaling of amount of released ACh by the number of presynaptic action potentials. Importantly, applying 20 μM (5*R*,6*R*)6-(3-propylthio-1,2,5-thiadiazol-4-yl)-1-azabicyclooctane (PTAC), an antagonist of $M_{1,3,5}$Rs[34], in the bath solution blocked the electrically evoked $\Delta F/F_0$ responses (**Supplementary Fig. 15**), indicating the detection of cholinergic signals.

We noted that at times, the minimal electrical stimulation-evoked fluorescence responses exhibited obvious spatial heterogeneity across subcellular regions of GACh2.0 expressing

Author Manuscript Author Manuscript Author Manuscript Author Manuscript

L2 stellate neurons. Analysis of the evoked fluorescence responses revealed one or a few subcellular hot spots, or regions of interest (ROIs), with largest $\Delta F/F_0$ responses, whereas other ROIs had smaller or undetectable changes in $\Delta F/F_0$ (**Fig. 4l-n**), suggesting the spatially-restricted release and clearance of ACh. Plotting $\Delta F/F_0$ responses at all ROIs against the distance from the ROI with largest $\Delta F/F_0$ responses yielded a volume transmission spread length constant of 9.0 μm for MEC L2 stellate neurons (**Fig. 4n**). To verify this surprisingly small cholinergic volume transmission, we examined the minimal electrical stimulation-evoked local fluorescence responses along the somatodendritic axis of GACh2.0 expressing hippocampal CA1 neurons (**Supplementary Fig. 16a**). Consistent with previous studies[29], we found that electrical stimuli of the stratum-oriens and pyramidale were most likely to elicit cholinergic responses in CA1 neurons (**Supplementary Fig. 16b,c**). The largest fluorescence responses were typically observed at one or a few subcellular ROIs in the soma of GACh2.0 expressing neurons, whereas fluorescence responses at other ROIs in the soma and dendrite of the same neurons were much smaller or undetectable (**Supplementary Fig. 16b,c**). Similar analysis gave a volume transmission spread length constant of 15.6 μm for CA1 neurons (**Supplementary Fig. 16d**). As a control, bath application of ACh induced similar $\Delta F/F_0$ responses along the somatodendritic axis of GACh2.0 expressing CA1 neurons (**Supplementary Fig. 16e**), ruling out the non-specific effect of unequal expression.

To determine whether GACh sensors may report other ACh release modes, we studied neurons in the medial habenula (**MHb**), which potentially release ACh during high frequency firing[8, 35]. GACh2.0 sensors were successfully expressed in IPN by AAV, and in close proximity with MHb cholinergic fibers, verified by post hoc ChAT immunostaining (**Supplementary Fig. 17a-c; Online Methods**). Two-photon imaging of GACh2.0 expressing neurons showed that brief 1-, 10-, 20- or 50-Hz 5-second electrical stimuli evoked no detectable fluorescence changes, whereas 100-Hz stimuli elicited small $\Delta F/F_0$ responses (**Supplementary Fig. 17e,g**). Bath application of GABA or $GABA_B$ receptor agonist baclofen enhanced $\Delta F/F_0$ responses in a frequency-dependent manner, consistent with our previous finding[35]. In contrast, saclofen, a $GABA_B$ receptor antagonist, reversed the potentiation effect. Moreover, Tio application completely abolished the $\Delta F/F_0$ responses, while donepezil, an acetylcholinesterase inhibitor[36], prolonged the potentiated $\Delta F/F_0$ responses (**Supplementary Fig. 17d, f, h-k**). These findings support the notion that extracellular GABA in IPN can drive habenula neurons firing in the physiological frequency range (up to 10–25 Hz[37]) to release ACh, which may be critical for fear control[35].

To rule out any non-specific effects that might be caused by long-term *in vivo* expression, we made chronic AAV expression of GACh2.0 in the dentate gyrus of hippocampus and examined the high K^+-evoked calcium responses with Cal590. High K+ elicited the same Cal590 fluorescence responses, compared to control non-expressing neurons (**Supplementary Fig. 18**), suggesting no non-specific effect from chronic GACh2.0 expression. Moreover, we made acute cortical slices after chronic *in vivo* lentiviral expression of GACh2.0 in barrel cortical L5 pyramidal neurons in mice. Simultaneous patch-clamp recordings showed that GACh2.0 expressing and control non-expressing L5 pyramidal neurons displayed the same resting membrane potential, input resistance,

Author Manuscript Author Manuscript Author Manuscript Author Manuscript

membrane time constant and average spiking frequency, as well as AMPA, NMDA and GABAergic responses, and paired pulse facilitation of AMPA responses (**Supplementary Fig. 19**).

We further examined the feasibility of optogenetic activation and optical imaging of cholinergic transmission simultaneously. We expressed DIO-oChIEF-tdTomato AAV in BF of ChAT-Cre mice for three weeks, followed by Sindbis viral expression of GACh2.0 in MEC L2 stellate neurons for 18 hours before preparing acute entorhinal cortical slices. We used single-photon laser pulses (470 nm) to optogenetically stimulate oChIEF-expressing cholinergic fibers in MEC, and simultaneously used two-photon laser scanning (950 nm), which is insufficient to activate oChIEF-expressing fibers[38], to image fluorescence responses in GACh2.0 expressing stellate neurons in MEC (**Supplementary Fig. 20a**). Twenty 5-ms laser pulses (at 1 Hz) elicited consistent fluorescence responses in GACh2.0 expressing neurons, which were largely blocked by bath application of 20 μM PTAC (**Supplementary Fig. 20b,c**).

GACh sensors in non-neuronal tissues

ACh released from parasympathetic nerve terminals in the pancreas and adrenal is critical for insulin secretion39 and stress/blood pressure regulation[40], respectively. We made Sindbis viral expression of GACh2.0 in the mouse pancreas and adrenal *in vivo*, and imaged fluorescence responses of GACh2.0 expressing cells in acutely prepared pancreas and adrenal gland tissue slices (**Supplementary Figs. 21** and **22**). Single electrical stimulations of local parasympathetic cholinergic fibers evoked evident fluorescence responses in GACh2.0 expressing pancreatic and adrenal cells (**Supplementary Figs. 21b,c** and **22b,c; Supplementary movies 6** and **7**). Increasing the number of stimulation pulses delivered at 2 Hz progressively increased the amplitude of $\Delta F/F_0$ responses in pancreatic cells, while the responses plateaued with >10 pulses in adrenal cells (**Supplementary Figs. 21d,e** and **22d,e**). Bath application of 20 μM PTAC blocked $\Delta F/F_0$ responses in GACh2.0 expressing pancreatic and adrenal cells (**Supplementary Figs. 21f,g** and **22f,g**), confirming the cholinergic signals.

GACh sensors in transgenic Drosophila in vivo

Next, we tested whether GACh sensors detect cholinergic transmission in live *Drosophila*. We created UAS-GACh1.0 and -GACh2.0 transgenic flies, and crossed them with a GH146-Gal4 driver line[41] to selectively express GACh1.0 and GACh2.0 in antennal lobe projection neurons, which receive abundant cholinergic inputs from olfactory receptor neurons[42]. Two-photon imaging revealed that application of the odorant isoamyl acetate (IA) induced region-specific and dose-dependent $\Delta F/F_0$ responses in DM2 glomerulus, but not DA1 glomerulus (**Fig. 5a-e;** cf.[43, 44]). Application of the odor solvent, mineral oil alone did not evoke $\Delta F/F_0$ changes in transgenic flies (**Fig. 5b,c**). As expected, IA-evoked $\Delta F/F_0$ responses in GACh2.0 transgenic flies were ~2-fold larger than those in GACh1.0 transgenic flies (**Fig. 5d,e**). Similarly, another odorant benzaldehyde also evoked region-specific and dose-dependent $\Delta F/F_0$ responses in the antennal lobe (**Supplementary Fig. 23a-d**). Moreover, IA elicited $\Delta F/F_0$ responses in the lateral horn, a higher-order olfactory center of *Drosophila* as well (**Supplementary Fig. 23e-g**). Using the spectrum non-overlapping red Ca^{2+} indicator

Author Manuscript Author Manuscript Author Manuscript Author Manuscript

RGECO[45], we re-examined IA-induced responses in control GH146 > RGECO and GH146 > GACh1.0/2.0,RGECO transgenic flies. Application of IA induced the same Ca2+ transients in the DM2 glomerulus in control GH146 > RGECO, GH146 > GACh1.0,RGECO and GH146 > GACh2.0,RGECO transgenic flies (**Supplementary Fig. 24**), again ruling out the non-specific effect from GACh expression.

GACh sensors in mouse visual cortex in vivo

Finally, we tested the performance of GACh sensors by two-photon imaging in awake mouse L2/3 visual cortex (**Fig. 6a; Online Methods;** cf.[46]). We used a video monitor to deliver a visual stimulation consisting of 10-s images of expanding white-filled circles, which was designed to elicit both attentional and visual responses ideal to trigger ACh release *in vivo*[47–50]. The 10-s visual stimulation, but not the following 50-s darkness, reliably induced sustained fluorescence responses in some GACh expressing neurons (**Fig. 6b-d**). However, some nearby expressing neurons exhibited no fluorescence responses to the same visual stimulation (**Fig. 6b,c**), suggesting a possible spatially specific visual stimulation-evoked ACh release *in vivo* (cf. **Fig. 5** and **Supplementary Fig. 16**).

DISCUSSION

In this study, we have developed and validated a family of genetically-encoded fluorescent ACh probes, GACh sensors. GACh sensors have the sensitivity, ligand specificity, SNR, kinetics and photostability suitable for monitoring cholinergic signals in diverse tissue preparations *in vitro*, *ex vivo* and *in vivo*. As with GCaMP3[51] and iGluSnFR[52], the $\Delta F/F_0$ responses of GACh sensors in intact tissues are smaller than in cultured cells, presumably attributable to the higher tissue background/basal fluorescence. We also noted that GACh sensors have a weak coupling to downstream G protein intracellular signaling in cultured cells, yet this coupling has no detectable effect on basic membrane properties, synaptic properties and cholinergic transmission in rodent neurons *in vitro* and *in vivo*, as well as sensory input-evoked cholinergic responses in *Drosophila in vivo*.

Central cholinergic neurons exhibit multiple distinct action potential firing patterns[32, 33, 37], yet the functional significance of these firing patterns remains elusive. Here we report that BF cholinergic neurons use low frequency 0.5−2 Hz tonic firing to generate large plateau-like postsynaptic ACh signals, and 8−12 Hz theta rhythmic phasic firing to elicit small transient postsynaptic ACh signals. A possible explanation is the high-frequency activation of cholinergic fibers may be more effective in recruiting presynaptic auto-receptor inhibition mechanism to suppress ACh release[53], which yielded more transient ACh signals. On the other hand, habenula neurons can fire high frequency action potentials of up to 10−25 Hz37. The firing triggers co-release of ACh with its primary neurotransmitter glutamate when a presynaptic $GABA_BR$-mediated potentiation mechanism is engaged. Although detailed aspects of cholinergic regulations remain to be worked out, our data are consistent with the view that presynaptic regulatory mechanisms may play key roles in governing release modes in central cholinergic transmission.

Another unresolved question concerns cholinergic volume transmission; whether ACh acts globally affecting a large number of neurons or mediates spatially restricted volume

Author Manuscript Author Manuscript Author Manuscript Author Manuscript

transmission remains a matter of debate[1–3, 13]. Directly visualizing the spread of released ACh in the hippocampus and MEC has allowed us to estimate the spread length constant of central cholinergic transmission, which ranges ~9–15 μm. Because the minimal electrical stimulation may activate multiple ACh release sites, this value is likely to be overestimated. Nevertheless, the estimation provides the first suggestion that central cholinergic transmission may have single-cell or subcellular specificity. Since G-protein-coupled receptors may relay postsynaptic signaling in a highly spatially restricted manner[54], it is tempting to speculate that intercellular cholinergic signal communication can achieve a subcellular precision. Together, the findings of fine firing frequency-controlled release and spatially restricted volume transmission advance our fundamental understanding of the regulation and precision of cholinergic signaling.

GACh sensors, which allow visualization of ACh signals in animal models *ex vivo* and *in vivo*, should advance our understanding of the pathogenesis of various diseases. For example, cholinergic signals are essential for high-level cognitive functions, including learning and memory, and dysregulation of cholinergic transmission is linked with various neurological disorders, including Alzheimer's disease. Yet, the cholinergic hypothesis-based acetylcholinesterase inhibitor treatment, the only available therapy for Alzheimer's disease[55], has limited efficacy and is far from ideal[36, 56]. Further understanding of central cholinergic transmission in physiological and pathological conditions is central to development of effective therapeutic strategies for Alzheimer's disease and other neurological diseases. Moreover, defective cholinergic signals have been implicated in the pathophysiology and treatment of a number of other non-neurological diseases[5–7], including diabetes[39], cardiovascular diseases[40], inflammation[59] and tumorigenesis[60]. We show here that GACh sensors are effective in monitoring cholinergic transmission in non-neuronal cells as well, including the pancreas and adrenal, thus endorsing the use of this tool to unravel the cholinergic mechanisms underlying these pathological conditions.

ONLINE METHODS

Animal preparation

Male and female Sprague-Dawley rats, and wild type and ChAT-Cre transgenic C57BL/6 mice were used to prepare cultured neurons, cultured hippocampal slices, acute brain slices, acute pancreas and adrenal slices in this study. Animals were maintained in the animal facilities at the Peking University, the National Institute of Biological Sciences, Beijing, China, University of Southern California, Stony Brook University or the University of Virginia, and family or pair housed in the temperature-controlled animal room with 12-h/12-h light/dark cycle. All procedures for animal surgery and maintenance were performed following protocols approved by the Animal Care & Use Committee of the Peking University, the National Institute of Biological Sciences, Beijing, China, University of Southern California, Stony Brook University or the University of Virginia and in accordance with US National Institutes of Health guidelines.

Author Manuscript Author Manuscript Author Manuscript Author Manuscript

Preparations of cultured cells, cultured neurons and cultured slices

HEK293T were cultured in DMEM (Gibco, MA) with 10% FBS (North TZ-Biotech Develop Co., Ltd, Beijing, China) at 37 °C, 5% CO_2, and passed to 12-mm glass coverslips in 24 well plates. Rat cortical neurons were prepared from postnatal 1-day old (P1) Sprague-Dawley rats as previously described[61]. Briefly, rat brains were dissected and digested by 0.25% Trypsin-EDTA (Gibco), and placed onto poly-D-lysine (Sigma-Aldrich, MO) coated coverslips with density of $0.5–1\times10^{6}$ cells/ml.

Cultured slices were prepared from P6–7 rats or mice following our previous studies[62, 63]. In brief, the hippocampi were dissected out in ice-cold HEPES-buffered Hanks' solution (pH 7.35) under sterile conditions, sectioned into 400 μm slices on a tissue chopper, and explanted onto a Millicell-CM membrane (0.4-μm pore size; Millipore, MA). The membranes were then placed in 750 μl of MEM culture medium, contained (in mM): HEPES 30, heat-inactivated horse serum 20%, glutamine 1.4, D-glucose 16.25, $NaHCO_3$ 5, $CaCl_2$ 1, $MgSO_4$ 2, insulin 1 mg/ml, ascorbic acid 0.012% at pH 7.28 and osmolarity 320. Cultured slices were maintained at 35°C, in a humidified incubator (ambient air enriched with 5% CO_2).

Preparations of acute tissue slices

Acute thalamic, barrel cortical, entorhinal cortical, hippocampal and MHb-fr-IPN brain slices, pancreas and adrenal tissues slices were prepared from P25–60 animals deeply anesthetized by xylazine-ketamine or pentobarbital (100 mg/kg) as described in our previous reports [63, 64]. The animals were decapitated and the brain block containing the thalamus, barrel cortex, MEC and/or hippocampus, the pancreas, or the adrenal was quickly removed and placed into cold (0–4°C) oxygenated physiological solution containing (in mM): 125 NaCl, 2.5 KCl, 1.25 NaH_2PO_4, 25 $NaHCO_3$, 1 $MgCl_2$, 25 dextrose, and 2 $CaCl_2$, pH 7.4. The brain blocks were directly sectioned into 400-μm-thick brain slices using a DSK microslicer (Ted Pella Inc.), while the pancreas and adrenal were first embedded in low-melting temperature agar (2.5% in BBS) and then sectioned into 400-μm-thick tissue slices[65]. For the MHb-fr-IPN slice preparation, the brains were first blocked at ~45° angle from the horizontal plane and then sectioned into 250-μm-thick slices by VT1200 vibratome (Leica, Germany). The tissue slices were kept at 37.0 ± 0.5 °C in oxygenated physiological solution for ~0.5–1 hour before imaging. During the recording and/or imaging the slices were submerged in a chamber and stabilized with a fine nylon net attached to a platinum ring. The recording chamber was perfused with oxygenated physiological solution. The half-time for the bath solution exchange was ~6 s, and the temperature of the bath solution was maintained at 34.0 ± 0.5 °C. All antagonists were bath applied. Distinct cell types, including L2 stellate neurons and L1 interneurons in MEC[66], L5 pyramidal neurons in the barrel cortex of mice[63, 67, 68], GABAergic thalamic reticular neurons and glutamatergic thalamocortical neurons in the ventral basal nucleus of rats[63, 69], could be easily identified under transmitted light illumination based on their locations and somatodendrtic morphology as characterized in the previous reports.

Author Manuscript Author Manuscript Author Manuscript Author Manuscript

Molecular biology

Molecular cloning was typically carried out using the Gibson assembly[70] with ~30-overlapping base primers and the Phusion DNA polymerase (New England Biolabs, MA), and verified by Sanger sequencing using in an in-house facility (sequencing platform in the School of Life Sciences of the Peking University). The chimeric GACh constructs were generated by subcloning full-length human GPCR cDNAs (hORFeome database8.1, the Dana-Farber Cancer Institute Center for Cancer Systems Biology) into the pDisplay vector (Invitrogen, MA), with an IgK leader sequence inserted before the coding region. The site-directed mutagenesis of the sequences of the two- and five-amino acid linkers in the N and C termini of cpGFP was made using primers containing various lengths of trinucleotides NNB (20 possible amino acids, Sangon Biotech, Shanghai, China). The applicable GACh sensors were then subcloned into the Sindbis viral vector, the lentiviral vector, or the AAV package vector under the human synapsin promoter to ensure the neuronal expression. To create the transgenic *Drosophila*, fragments of GACh sensors including the IgK leader sequence were cloned into the pUAST vector, and subsequently injected into *Drosophila* embryo following a standard protocol (Fungene biotechnology, Beijing). To report the receptor endocytosis, super-ecliptic pHluorin[71] was cloned to the N terminus of M_3R, with a three amino acid linker (GGA) to ensure correct protein folding and trafficking.

Expression of GACh sensors and other recombinant proteins

HEK293T cells were typically transfected using the PEI method (with a typical ratio of 1 μg DNA to 4 μg PEI), media replaced 4–6 hours later, and cells imaged 24 hours later. Cultured neurons were transfected after 7–9 days *in vitro* using the calcium phosphate transfection method and experiments were performed 48 hours after transfection. Neurons in hippocampal cultured slices were infected after 8−18 days *in vitro* with lentivirus or Sindbis virus, and then incubated on culture media and 5% CO_2 before experiments. For *in vivo* expression, P28−84 animals were initially anesthetized by an intraperitoneal injection of 2,2,2-Tribromoethanol (Avetin, 500 mg/kg) or ketamine and xylazine (10 and 2 mg/kg, respectively), and then placed in a stereotaxic frame. In some of the animals, AAV of GACh sensors (with a titer of $>10^{12}$/ml) was injected into IPN with a microsyringe pump (Nanoliter 2000 Injector, WPI) using the coordinates (AP: −3.13 mm from Bregma; DV: −4.95 mm; ML: 1.33 mm with 15° angle towards the midline), or into the dentate gyrus of hippocampus (AP: −1.80 mm from Bregma; DV: −1.80 mm; ML: 0.80 mm). In other animals, a glass pipette was used to penetrate into the thalamic ventrobasal nucleus, thalamic reticular nucleus, the barrel cortex and MEC according to stereotaxic coordinates, or the dissected pancreas and adrenal, to deliver ~50 nl of viral solution by pressure injection to infect neurons, or pancreas and adrenal cells with GACh sensors. In ChAT-Cre transgenic mice, AAV of DIO-oChIEF-tdTomato was first injected into BF according to the previously described coordinates[72], and three weeks later, Sindbis virus of GACh sensors was injected into MEC for ~18 hours before preparing acute brain slices for experiments.

Electrophysiology

Simultaneous dual whole-cell recordings were obtained from two nearby infected and non-infected hippocampal CA1 pyramidal neurons under visual guidance using fluorescence and

Author Manuscript Author Manuscript Author Manuscript Author Manuscript

transmitted light illumination[63, 64]. The patch recording pipettes (4–7 MΩ) were filled with intracellular solution containing 115 mM cesium methanesulfonate, 20 mM CsCl, 10 mM HEPES, 2.5 mM $MgCl_2$, 4 mM Na_2ATP, 0.4 mM Na_3GTP, 10 mM sodium phosphocreatine, 0.6 mM EGTA, and 0.1 mM spermine and 0.5% biocytin (pH 7.25) for voltage-clamp recordings, or containing 120 mM potassium gluconate, 4 mM KCl, 10 mM HEPES, 4 mM MgATP, 0.3 mM Na_3GTP, 10 mM sodium phosphocreatine and 0.5% biocytin (pH 7.25) for current-clamp recordings. Bath solution (29 ± 1.5 ºC) contained (in mM): NaCl 119, KCl 2.5, $CaCl_2$ 4, $MgCl_2$ 4, $NaHCO_3$ 26, NaH_2PO_4 1, glucose 11, picrotoxin (PTX) 0.1, bicuculline 0.01, and 2-chloroadenosine 0.002, at pH 7.4 and gassed with 5% CO_2/95% O_2. PTX was excluded when GABA responses were examined. Whole-cell recordings were made with up to two Axoclamp 2B or Axopatch-200B patch clamp amplifiers (Molecular Devices, Sunnyvale, CA). Junction potentials were not corrected. Synaptic responses were evoked by bipolar electrodes with single voltage pulses (200 μs, up to 20 V). Synaptic AMPA and NMDA responses at −60 mV and +40 mV or GABA responses at 0 mV were averaged over 90 trials. To minimize the effect from AMPA responses, the peak NMDA responses at +40 mV were measured after digital subtraction of estimated AMPA responses at +40 mV. Cholinergic fibers in tissue slices were stimulated with a bipolar electrode placed ~50–200 μm from imaged cells with single or a train of voltage pulses (500 μs, up to 50 V) to evoke ACh release.

Fluorescence imaging of cultured cells and neurons

In some experiments, the fluorescence signals of HEK293T cells transfected with the muscarinic receptor-based chimeric constructs were measured with a TECAN Safire2 fluorescence plate reader (TECAN, Männedorf, Switzerland; excitation, 480 nm; emission, 520 nm). During the measurement, the culture media was replaced with 100 μl Tyrode solution containing ACh at varied concentrations from 0–100 μM. The $\Delta F/F_0$ of each construct was obtained by averaging the ACh-induced fluorescence responses of transfected wells after digitally subtracting that of neighboring control non-transfected wells.

In other culture cell experiments, HEK293T cells and cultured neurons were imaged by an inverted Nikon Ti-E A1 confocal microscope with a 40×/1.35 NA oil objective (Nikon, Tokyo, Japan). Cells were perfused with standard extracellular Tyrode solution containing (in mM): 150 NaCl, 4 KCl, 2 $MgCl_2$, 2 $CaCl_2$, 10 HEPES and 10 Glucose, with pH of 7.4, in an imaging chamber during imaging. Agonist acetylcholine (Solarbio, Beijing, China), tiotropium bromide (Dexinjia Bio & Tech Co., Ltd, Jinan, China), and AF-DX 384 (Sigma-Aldrich) were delivered with a custom-made perfusion system and/or bath applied. The chamber was washed with Tyrode solution between applications and cleaned with 75% ethanol between experiments.

Fluorescence imaging of cells in cultured and acute slice preparations

Wide field epifluorescence imaging was performed using Hamamatsu ORCA FLASH4.0 camera (Hamamatsu Photonics, Japan), and GACh expressing cells in cultured hippocampal slices and acutely prepared brain slices are excited by a 460-nm ultrahigh-power low-noise LED (Prizmatix, Givat-Shmuel, Israel). The frame rate of FLASH4.0 camera was set to 10 Hz. To synchronize image capture with drug perfusion, electrical stimulation, and/or

Author Manuscript Author Manuscript Author Manuscript Author Manuscript

electrophysiological recording, the camera was set to external trigger mode and triggered by a custom-written IGOR Pro 6 program (WaveMetrics, Lake Oswego, OR). Agonists or antagonists, including acetylcholine and atropine (Sigma-Aldrich), and nicotine, oxotremorine M, PTAC and TMPH (Tocris Bioscience, Bristol, UK), were either bath applied or puff applied with a glass pipette (~1 μm in tip diameter) positioned ~150 μm above the imaged neurons using 500-ms 30-kPa pressure pulses.

Two-photon imaging was performed using a custom-built microscope or an Olympus FV1000 microscope (for IPN experiments; Olympus, Japan). The parameters of frame scan were typically set at a size of 200 × 200 pixels and a speed of 1 frame/s. For all optical experiments, the actual two-photon scanning time was set at ~700 ms/frame, and twenty 10-ms 470-nm blue M470F1 LED (Thorlabs, NJ) light pulses were synchronously delivered at 1 Hz during the ~300-ms frame scanning break periods to activate oChIEF-tdTomato expressing cholinergic fibers without interfering two-photon imaging. The blue light of the LED was fiber-coupled to an Ø200 μm fiber optic cannula positioned ~250 μm away from imaged neurons. The light power out of the cannula was set at 2 mW. The fluorescence of GACh2.0 was excited by a femtosecond Ti:Sapphire laser (Chameleon Ultra II, Coherent) at a wavelength of 950 nm. Changes in fluorescence were quantified as increases in fluorescence from baseline divided by resting fluorescence ($\Delta F/F_0$) and averaged for ~10 trials. To quantify surface expression of GACh sensors, lentiviral expression of GACh1.0, GACh1.5 or GACh2.0 was made in the CA1 region of organotypic hippocampal cultured slices. About ~1–2 weeks after expression, GACh expressing CA1 pyramidal neurons were patch-clamp recorded and loaded with 25 μM Alexa Fluor 594 (Life Technologies) for ~10 minutes, and two-photon images were then taken at different compartments along the apical dendrites. The multiple patch-clamp recordings, optogenetics, epifluorescence and two-photon imaging were typically operated by a single custom-written IGOR Pro 6 program (WaveMetrics, Lake Oswego, OR). To image the high KCl-induced calcium signals, 20 μM Cal590F (AAT Bioquest Inc., Sunnyvale, CA) was bath-loaded into hippocampal cells in acute slices and subsequently washed with ACSF for 30 minutes before imaging. Cal590 dye was excited with a two-photon laser at 950 nm, and 90 mM KCl was perfused to stimulate calcium signals.

Immunocytochemistry

Mice infected with GACh sensors were deeply anesthetized with pentobarbital (400 mg/kg; i.p.), and transcardially perfused first with cold normal saline and then 4% paraformaldehyde in 0.1 M PBS. Brain blocks were post-fixed for ≥4 hours, cryoprotected in 30% sucrose for ≥24 hours, then embedded in tissue freezing medium and sectioned into 50-μm-thick coronal sections with a freezing Leica CM 1900 microtome (Leica, Germany). To label cholinergic terminals from MHb and GACh expressing neurons in IPN, tissue sections were rinsed and immunoreacted with goat ChAT antibody (1:500, Millipore, #ab144p) and rabbit GFP antibody (1:500, Abcam, #ab6556), and then labeled with goat-anti-rabbit second antibody conjugated Alexa 488 and donkey-anti-goat second antibody conjugated Alexa 555 after extensive washing. The immunolabeled tissue sections were imaged with a confocal microscope.

Author Manuscript Author Manuscript Author Manuscript Author Manuscript

To recover the morphology of recorded neurons, the slices were fixed by immersion in 3% acrolein/4% paraformaldehyde in 0.1 M PBS at 4°C for 24 hours after *in vitro* patch-clamp recordings with internal solution containing additional 1% biocytin, and then processed with the avidin-biotin-peroxidase method to reveal cell morphology. The morphologically recovered cells were examined and reconstructed with the aid of a microscope equipped with a computerized reconstruction system Neurolucida (MicroBrightField, Colchester, VT).

Fluorescence imaging of transgenic Drosophila

Transgenic *Drosophila* lines with strong GACh expression levels and robust odor responses were chosen after crossing UAS-GACh1.0 and -GACh2.0 transgenic flies with a GH146-Gal4 driver line. They were reared at room temperature for 8~12 days on standard medium after eclosion before experiments. For imaging experiments, live flies were mounted and prepared as our previous study[73]. Briefly, animals were mounted to a small dish, with their rectangular patch of cuticle between the eyes, excessive fat bodies and air sacs surrounding the antennal lobe removed, and the pair of muscles underneath the proboscis cut to reduce the brain movement. Isoamyl acetate (Sigma-Aldrich; Cat# 306967) and benzaldehyde (Sinopharm Chemical Reagent Co., Ltd, Shanghai,China, Cat# 30017018) were initially diluted by 100-fold or 1000-fold (vol/vol) in mineral oil (Sigma-Aldrich; Cat# 69794) and then placed in a glass bottle (100 μl in 900 μl mineral oil), delivered at 200 ml/min, and mixed with purified air (1000 ml/min). The mixed air stream was presented to flies through a 1-cm-wide opening Teflon tube placed ~1 cm from their antennas, and controlled by a Teflon solenoid valves and synchronized with the image acquisition system by Arduino boards. Imaging was made using a commercial Olympus BX61WI two-photon microscope with a 25×/NA: 1.05 water-immersion objective and a mode-locked Ti:Sapphirelaser (Mai tai) tuned to 950 nm. The Glomeruli were identified according to the previous established antennal lobe map[74].

Fluorescence imaging of behaving mice

Mice were initially anesthetized to remove the head skin to attach a metal recording chamber, followed by a 3−5-day recovery and another 2−5-day head-fixation habituation. The animals were then anesthetized again to open the skull above the primary visual cortex (centered ~2.5 lateral, ~1.5 mm anterior from lambda) to pressure inject ~100 nl of Sindbis virus of GACh2.0 or AAV viruses of hsyn-tTA and TRE-GACh2.0 (with a 1:1 mix ratio; a speeded AAV expression approach[75]). The craniotomy was completed by fitting a cranial window made with a 3-mm circular or a 2 × 2 mm square #2 coverslip. About 16 hours after the surgery, the animals were head-fixed on a circular treadmill and imaged using a custom-built 2-photon system powered with an InSight DS+ laser (Spectra Physics) and operated with ScanImage 5.1 software[76]. Images were acquired from individual cells (or small groups of cells when possible) continuously at either 30 Hz (512 × 512 pixels) or 60 Hz (256 × 256 pixels). The mouse was shown a stimulus consisting of 50 seconds of darkness followed by 10 seconds of expanding white circles appearing at random positions on the screen. All data analysis was done in Matlab (Mathworks). Automatic image alignment was validated by manual inspection. ROIs were manually drawn over the cell bodies and raw fluorescent traces were extracted. Fluorescent traces were filtered by a 2 second moving average window to reduce fluctuations, and divided into 10 second segments corresponding to either

Author Manuscript Author Manuscript Author Manuscript Author Manuscript

periods of darkness or periods of visual stimulation and the maximum $\Delta F/F_0$ was compared for periods with or without stimulation.

Statistical analysis

Statistical results were reported as mean ± s.e.m. Animals were randomly assigned into control or experimental groups and investigators were blinded to experiment treatments. Given the negative correlation between the variation and square root of sample number, *n*, the group sample size was typically set to be ~10–25 to optimize the power of statistical tests and efficiency. Statistical significances of the means ($p < 0.05$; two sides) were determined using Wilcoxon and Mann-Whitney Rank Sum non-parametric tests for paired and unpaired samples, respectively. Statistical significances of the linear relationships of two data groups were determined using linear regression *t* tests provided the normality and constant variance tests passed.

Supplementary Material

Refer to Web version on PubMed Central for supplementary material.

Acknowledgments:

We thank Dr. Loren Looger and colleagues for sharing their unpublished acetylcholine sensors that validated some of our results. We thank Y. Rao for generous sharing of two-photon microscopy. We are also grateful to L. Luo, S. Owen, Y. Rao and L. Nevin for critical reading of the manuscript. We thank Z. Ye for the help in art designing. This work was supported by the National Basic Research Program of China (973 Program; grant 2015CB856402), The General Program of National Natural Science Foundation of China (project 31671118 and project 31371442), and the Junior Thousand Talents Program of China to Y.L. Additional support comes from NIH grants NS103558 (Y.L. and L.I.Z.), DC008983 (L.I.Z.), MH104227 and MH109475 (Y.Z.), MH109104 and NS022061 (L.W.R.), LH089717 (P.Q.B.), and NS053570, NS091452, NS094980, NS092548 and NS104670 (J.J.Z.). J.J.Z. is the Radboud Professor and Sir Yue-Kong Pao Chair Professor.

REFERENCES:

1. Ballinger EC , Ananth M , Talmage DA & Role LW Basal forebrain cholinergic circuits and signaling in cognition and cognitive decline. Neuron 91, 1199–1218 (2016). [PubMed: 27657448]
2. Picciotto MR , Higley MJ & Mineur YS Acetylcholine as a neuromodulator: cholinergic signaling shapes nervous system function and behavior. Neuron 76, 116–129 (2012). [PubMed: 23040810]
3. Dani JA & Bertrand D Nicotinic acetylcholine receptors and nicotinic cholinergic mechanisms of the central nervous system. Annual review of pharmacology and toxicology 47, 699–729 (2007).
4. Dineley KT , Pandya AA & Yakel JL Nicotinic ACh receptors as therapeutic targets in CNS disorders. Trends in pharmacological sciences 36, 96–108 (2015). [PubMed: 25639674]
5. Kruse AC et al. Muscarinic acetylcholine receptors: novel opportunities for drug development. Nature reviews. Drug discovery 13, 549–560 (2014). [PubMed: 24903776]
6. Soreq H Checks and balances on cholinergic signaling in brain and body function. Trends in neurosciences 38, 448–458 (2015). [PubMed: 26100140]
7. Wessler I & Kirkpatrick CJ Acetylcholine beyond neurons: the non-neuronal cholinergic system in humans. British journal of pharmacology 154, 1558–1571 (2008). [PubMed: 18500366]
8. Ren J et al. Habenula “cholinergic” neurons co-release glutamate and acetylcholine and activate postsynaptic neurons via distinct transmission modes. Neuron 69, 445–452 (2011). [PubMed: 21315256]
9. Williams MJ & Adinoff B The role of acetylcholine in cocaine addiction. Neuropsychopharmacology : official publication of the American College of Neuropsychopharmacology 33, 1779–1797 (2008). [PubMed: 17928814]

Author Manuscript Author Manuscript Author Manuscript Author Manuscript

10. Francis PT , Palmer AM , Snape M & Wilcock GK The cholinergic hypothesis of Alzheimer's disease : a review of progress. 137–147 (1999).
11. Vita JA et al. Coronary Vasomotor Response to Acetylcholine Relates to Risk Factors for Coronary Artery Disease. 491–498 (1989).
12. Dang N , Meng X & Song H Nicotinic acetylcholine receptors and cancer (Review). 515–518 (2016).
13. Sarter M , Parikh V & Howe WM Phasic acetylcholine release and the volume transmission hypothesis: time to move on. Nature reviews. Neuroscience 10, 383–390 (2009). [PubMed: 19377503]
14. Kodama T , Lai YY & Siegel JM Enhancement of acetylcholine release during REM sleep in the caudomedial medulla as measured by in vivo microdialysis. Brain research 580, 348–350 (1992). [PubMed: 1504813]
15. Schuvailo ON et al. Carbon fibre-based microbiosensors for in vivo measurements of acetylcholine and choline. Biosensors & bioelectronics 21, 87–94 (2005). [PubMed: 15967355]
16. Barnea G et al. The genetic design of signaling cascades to record receptor activation. Proceedings of the National Academy of Sciences of the United States of America 105, 64–69 (2008). [PubMed: 18165312]
17. Ziegler N , Batz J , Zabel U , Lohse MJ & Hoffmann C FRET-based sensors for the human M1-, M3-, and M5-acetylcholine receptors. Bioorganic & medicinal chemistry 19, 1048–1054 (2011). [PubMed: 20716489]
18. Markovic D et al. FRET-based detection of M1 muscarinic acetylcholine receptor activation by orthosteric and allosteric agonists. PloS one 7, e29946 (2012). [PubMed: 22272263]
19. Muller A , Joseph V , Slesinger PA & Kleinfeld D Cell-based reporters reveal in vivo dynamics of dopamine and norepinephrine release in murine cortex. Nature methods 11, 1245–1252 (2014). [PubMed: 25344639]
20. Nguyen QT et al. An in vivo biosensor for neurotransmitter release and in situ receptor activity. Nature neuroscience 13, 127–132 (2010). [PubMed: 20010818]
21. Lin MZ & Schnitzer MJ Genetically encoded indicators of neuronal activity. Nature neuroscience 19, 1142–1153 (2016). [PubMed: 27571193]
22. Kruse AC et al. Activation and allosteric modulation of a muscarinic acetylcholine receptor. Nature 504, 101–106 (2013). [PubMed: 24256733]
23. Rasmussen SG et al. Crystal structure of the human beta2 adrenergic G-protein-coupled receptor. Nature 450, 383–387 (2007). [PubMed: 17952055]
24. Helassa N , Podor B , Fine A & Torok K Design and mechanistic insight into ultrafast calcium indicators for monitoring intracellular calcium dynamics. Scientific reports 6, 38276 (2016). [PubMed: 27922063]
25. Chen TW et al. Ultrasensitive fluorescent proteins for imaging neuronal activity. Nature 499, 295–300 (2013). [PubMed: 23868258]
26. Jakubik J , Bacakova L , El-Fakahany EE & Tucek S Positive cooperativity of acetylcholine and other agonists with allosteric ligands on muscarinic acetylcholine receptors. Molecular pharmacology 52, 172–179 (1997). [PubMed: 9224827]
27. Caulfield MP & Birdsall NJ International Union of Pharmacology. XVII. Classification of muscarinic acetylcholine receptors. Pharmacological reviews 50, 279–290 (1998). [PubMed: 9647869]
28. Papke RL et al. The effects of subunit composition on the inhibition of nicotinic receptors by the amphipathic blocker 2,2,6,6-tetramethylpiperidin-4-yl heptanoate. Molecular pharmacology 67, 1977–1990 (2005). [PubMed: 15761116]
29. Shen J & Barnes CA Age-related decrease in cholinergic synaptic transmission in three hippocampal subfields. Neurobiology of aging 17, 439–451 (1996). [PubMed: 8725906]
30. Eckenstein FP , Baughman RW & Quinn J An anatomical study of cholinergic innervation in rat cerebral cortex. Neuroscience 25, 457–474 (1988). [PubMed: 2456488]
31. Ray S et al. Grid-layout and theta-modulation of layer 2 pyramidal neurons in medial entorhinal cortex. Science 343, 891–896 (2014). [PubMed: 24457213]

Author Manuscript Author Manuscript Author Manuscript Author Manuscript

32. Simon AP , Poindessous-Jazat F , Dutar P , Epelbaum J & Bassant MH Firing properties of anatomically identified neurons in the medial septum of anesthetized and unanesthetized restrained rats. J Neurosci 26, 9038–9046 (2006). [PubMed: 16943562]
33. Duque A , Tepper JM , Detari L , Ascoli GA & Zaborszky L Morphological characterization of electrophysiologically and immunohistochemically identified basal forebrain cholinergic and neuropeptide Y-containing neurons. Brain structure & function 212, 55–73 (2007). [PubMed: 17717698]
34. Bymaster FP et al. Unexpected antipsychotic-like activity with the muscarinic receptor ligand (5R, 6R)6-(3-propylthio-1,2,5-thiadiazol-4-yl)-1-azabicyclo[3.2.1]octane. European journal of pharmacology 356, 109–119 (1998). [PubMed: 9774240]
35. Zhang J et al. Presynaptic excitation via $GABA_B$ receptors in habenula cholinergic neurons regulates fear memory expression. Cell 166, 716–728 (2016). [PubMed: 27426949]
36. Zemek F et al. Outcomes of Alzheimer's disease therapy with acetylcholinesterase inhibitors and memantine. Expert opinion on drug safety 13, 759–774 (2014). [PubMed: 24845946]
37. Zhao H & Rusak B Circadian firing-rate rhythms and light responses of rat habenular nucleus neurons in vivo and in vitro. Neuroscience 132, 519–528 (2005). [PubMed: 15802202]
38. Wang G et al. An optogenetics- and imaging-assisted simultaneous multiple patch-clamp recordings system for decoding complex neural circuits. Nature protocols 10, 397–412 (2015). [PubMed: 25654757]
39. Satin LS & Kinard TA Neurotransmitters and their receptors in the islets of Langerhans of the pancreas: what messages do acetylcholine, glutamate, and GABA transmit? Endocrine 8, 213–223 (1998). [PubMed: 9741825]
40. Ungar A & Phillips JH Regulation of the adrenal medulla. Physiological reviews 63, 787–843 (1983). [PubMed: 6308693]
41. Stocker RF , Heimbeck G , Gendre N & de Belle JS Neuroblast ablation in Drosophila P[GAL4] lines reveals origins of olfactory interneurons. Journal of neurobiology 32, 443–456 (1997). [PubMed: 9110257]
42. Wilson RI Early olfactory processing in Drosophila: mechanisms and principles. Annual review of neuroscience 36, 217–241 (2013).
43. Ng M et al. Transmission of olfactory information between three populations of neurons in the antennal lobe of the fly. Neuron 36, 463–474 (2002). [PubMed: 12408848]
44. Wang JW , Wong AM , Flores J , Vosshall LB & Axel R Two-photon calcium imaging reveals an odor-evoked map of activity in the fly brain. Cell 112, 271–282 (2003). [PubMed: 12553914]
45. Zhao Y et al. An expanded palette of genetically encoded Ca^{2+} indicators. Science 333, 1888–1891 (2011). [PubMed: 21903779]
46. Ibrahim LA et al. Cross-Modality Sharpening of Visual Cortical Processing through Layer-1-Mediated Inhibition and Disinhibition. Neuron 89, 1031–1045 (2016). [PubMed: 26898778]
47. Letzkus JJ et al. A disinhibitory microcircuit for associative fear learning in the auditory cortex. Nature 480, 331–335 (2011). [PubMed: 22158104]
48. Niell CM & Stryker MP Modulation of visual responses by behavioral state in mouse visual cortex. Neuron 65, 472–479 (2010). [PubMed: 20188652]
49. Hasselmo ME & Sarter M Modes and models of forebrain cholinergic neuromodulation of cognition. Neuropsychopharmacology : official publication of the American College of Neuropsychopharmacology 36, 52–73 (2011). [PubMed: 20668433]
50. Herrero JL et al. Acetylcholine contributes through muscarinic receptors to attentional modulation in V1. Nature 454, 1110–1114 (2008). [PubMed: 18633352]
51. Tian L et al. Imaging neural activity in worms, flies and mice with improved GCaMP calcium indicators. Nature methods 6, 875–881 (2009). [PubMed: 19898485]
52. Marvin JS et al. An optimized fluorescent probe for visualizing glutamate neurotransmission. Nature methods 10, 162–170 (2013). [PubMed: 23314171]
53. Alberts P , Bartfai T & Stjarne L The effects of atropine on [3H]acetylcholine secretion from guinea-pig myenteric plexus evoked electrically or by high potassium. The Journal of physiology 329, 93–112 (1982). [PubMed: 7143261]

Author Manuscript Author Manuscript Author Manuscript Author Manuscript

54. Sungkaworn T et al. Single-molecule imaging reveals receptor-G protein interactions at cell surface hot spots. Nature 550, 543–547 (2017). [PubMed: 29045395]
55. Mash DC , Flynn DD & Potter LT Loss of M_2 muscarine receptors in the cerebral cortex in Alzheimer's disease and experimental cholinergic denervation. Science 228, 1115–1117 (1985). [PubMed: 3992249]
56. Ashford JW Treatment of Alzheimer's disease: the legacy of the cholinergic hypothesis, neuroplasticity, and future directions. Journal of Alzheimer's disease : JAD 47, 149–156 (2015). [PubMed: 26402763]
57. Wess J , Eglen RM & Gautam D Muscarinic acetylcholine receptors: mutant mice provide new insights for drug development. Nature reviews. Drug discovery 6, 721–733 (2007). [PubMed: 17762886]
58. Gautam D et al. A critical role for beta cell M3 muscarinic acetylcholine receptors in regulating insulin release and blood glucose homeostasis in vivo. Cell metabolism 3, 449–461 (2006). [PubMed: 16753580]
59. Tracey KJ Reflex control of immunity. Nature reviews. Immunology 9, 418–428 (2009).
60. Magnon C et al. Autonomic nerve development contributes to prostate cancer progression. Science 341, 1236361 (2013). [PubMed: 23846904]
61. Zhang Q et al. The dynamic control of kiss-and-run and vesicular reuse probed with single nanoparticles. Science 323, 1448–1453 (2009). [PubMed: 19213879]
62. Qin Y et al. State-dependent Ras signaling and AMPA receptor trafficking. Genes & development 19, 2000–2015 (2005). [PubMed: 16107614]
63. Wang G et al. Cav3.2 calcium channels control NMDA receptor-mediated transmission: a new mechanism for absence epilepsy. Genes & development 29, 1535–1551 (2015). [PubMed: 26220996]
64. Lim CS et al. BRaf signaling principles unveiled by large-scale human mutation analysis with a rapid lentivirus-based gene replacement method. Genes & development 31, 537–552 (2017). [PubMed: 28404629]
65. Hu C , Rusin CG , Tan Z , Guagliardo NA & Barrett PQ Zona glomerulosa cells of the mouse adrenal cortex are intrinsic electrical oscillators. The Journal of clinical investigation 122, 2046–2053 (2012). [PubMed: 22546854]
66. Canto CB & Witter MP Cellular properties of principal neurons in the rat entorhinal cortex. II. The medial entorhinal cortex. Hippocampus 22, 1277–1299 (2012). [PubMed: 22161956]
67. Zhu JJ Maturation of layer 5 neocortical pyramidal neurons: amplifying salient layer 1 and layer 4 inputs by Ca^{2+} action potentials in adult rat tuft dendrites. J Physiol (Lond) 526, 571–587 (2000). [PubMed: 10922009]
68. Zhu JJ Activity level-dependent synapse-specific AMPA receptor trafficking regulates transmission kinetics. J Neurosci 29, 6320–6335 (2009). [PubMed: 19439609]
69. Zhu JJ & Uhlrich DJ Nicotinic receptor-mediated responses in relay cells and interneurons in the rat lateral geniculate nucleus. Neuroscience 80, 191–202. (1997). [PubMed: 9252231]
70. Gibson DG et al. Enzymatic assembly of DNA molecules up to several hundred kilobases. Nature methods 6, 343–345 (2009). [PubMed: 19363495]
71. Miesenböck G , De Angelis D.a. & Rothman JE Visualizing secretion and synaptic transmission with pH-sensitive green fluorescent proteins. Nature 394, 192–195 (1998). [PubMed: 9671304]
72. Jiang L et al. Cholinergic signaling controls conditioned fear behaviors and enhances plasticity of cortical-amygdala circuits. Neuron 90, 1057–1070 (2016). [PubMed: 27161525]
73. Liang L et al. GABAergic projection neurons route selective olfactory inputs to specific higher-order neurons. Neuron 79, 917–931 (2013). [PubMed: 24012005]
74. Laissue PP et al. Three-dimensional reconstruction of the antennal lobe in Drosophila melanogaster. The Journal of comparative neurology 405, 543–552 (1999). [PubMed: 10098944]
75. Liu B , Wang S , Brenner M , Paton JF & Kasparov S Enhancement of cell-specific transgene expression from a Tet-Off regulatory system using a transcriptional amplification strategy in the rat brain. The journal of gene medicine 10, 583–592 (2008). [PubMed: 18324737]

Author Manuscript Author Manuscript Author Manuscript Author Manuscript

76. Pologruto TA , Sabatini BL & Svoboda K ScanImage : Flexible software for operating laser scanning microscopes. 9, 1–9 (2003)

Author Manuscript
Author Manuscript
Author Manuscript
Author Manuscript

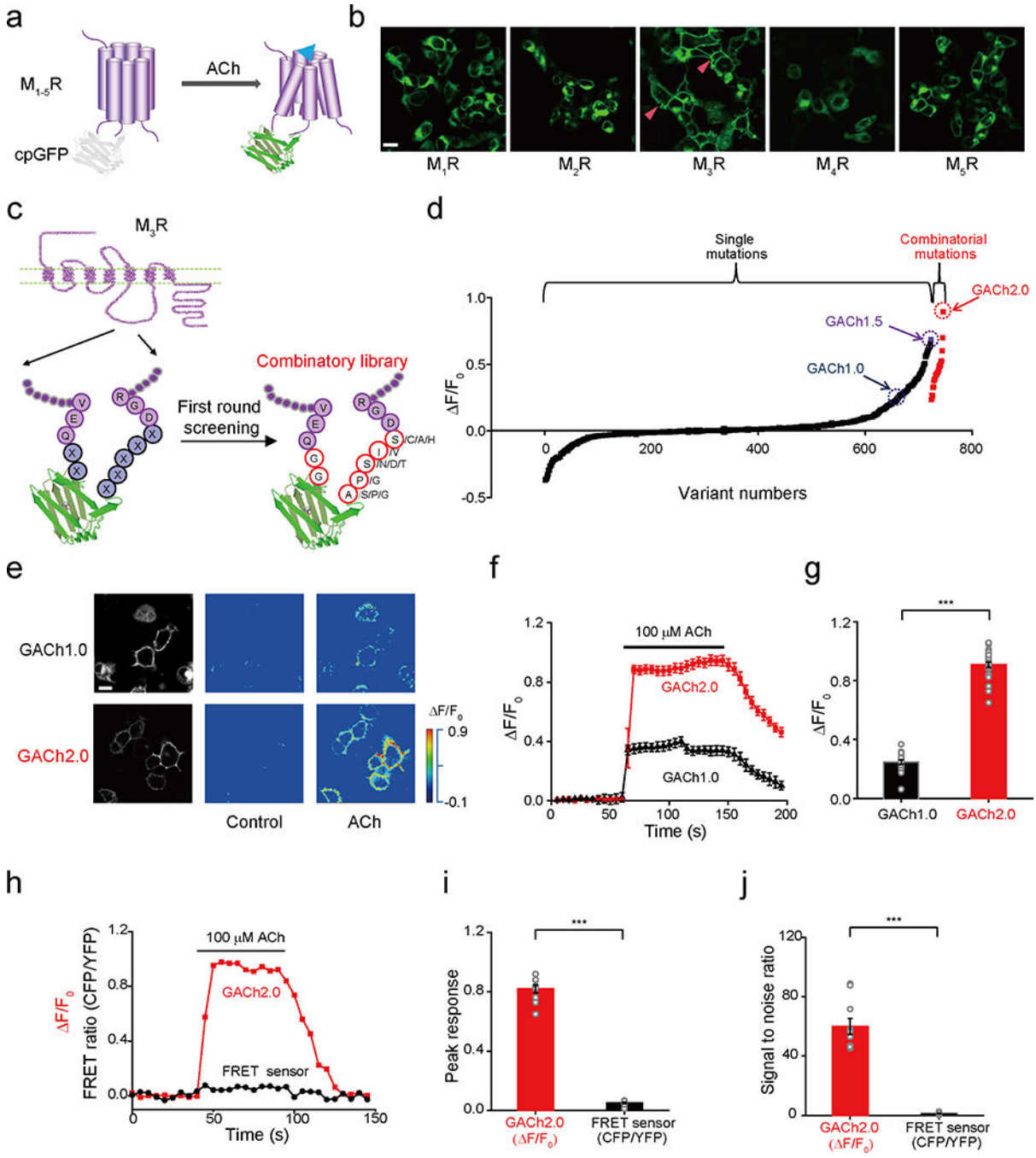

Figure 1. Development of GACh sensors.

(**a**) Schematic drawing shows the principle of the GPCR Activation Based ACh (GACh) sensor.

(**b**) Membrane expression of the different MR-based candidate GACh sensors in HEK293T cells. The red arrow head indicates membrane localized signals.

(**c**) Schematic drawing illustrates variants with one or multiple single-point mutations on the seven linker residues (total 18 hits).

Author Manuscript Author Manuscript Author Manuscript Author Manuscript

(**d**) Fluorescence responses of HEK293T cells expressing one of ~750 candidate GACh sensors harboring either randomized point or combinatorial mutations to the bath application of 100 μM ACh. Note $\Delta F/F_0$ of the combinatorial mutation-harboring GACh2.0 to be ~100% and data points are averaged responses of 2–10 cells.

(**e**) Fluorescence responses of GACh1.0 and GACh2.0 expressing cells to the bath application of ACh.

(**f-g**) $\Delta F/F_0$ of GACh1.0 and GACh2.0 expressing cells to ACh application (GACh1.0: 24.6 ± 1.5%, $n = 19$ cells from 5 cultures, GACh2.0: 90.1 ± 1.7%, $n = 29$ cells from 8 cultures, $U = 551$, $p = 6.72E\text{-}9$).

(**h**) Fluorescence responses of HEK293T cells expressing either GACh2.0 or M_1R-based FRET sensor to the application of ACh (100 μM).

(**i-j**) Averaged $\Delta F/F_0$ or ΔFRET ratio (GACh2.0: 94.0 ± 3.0%, $n = 10$ cells from 2 cultures; FRET: 6.61 ± 0.4%, $n = 10$ cells from 2 cultures, $U = 100$, $p = 1.09E\text{-}5$) and SNR (GACh2.0: 60.0 ± 5.4, $n = 10$ cells from 2 cultures; FRET: 1.12 ± 0.21, $n = 10$ cells from 2 cultures, $U = 100$, $p = 1.83E\text{-}4$) of GACh2.0 and M_1R-based FRET sensor expressing cells to ACh application.

Data are shown with mean ± s.e.m, with error bars indicating s.e.m. Experiments in (**b**) and (**e**) were repeated independently for more than 5 cultures with similar results.

***, $p < 0.001$ (Mann-Whitney Rank Sum non-parametric tests, two-sides). All scale bars, 10 μm.

Author Manuscript Author Manuscript Author Manuscript Author Manuscript

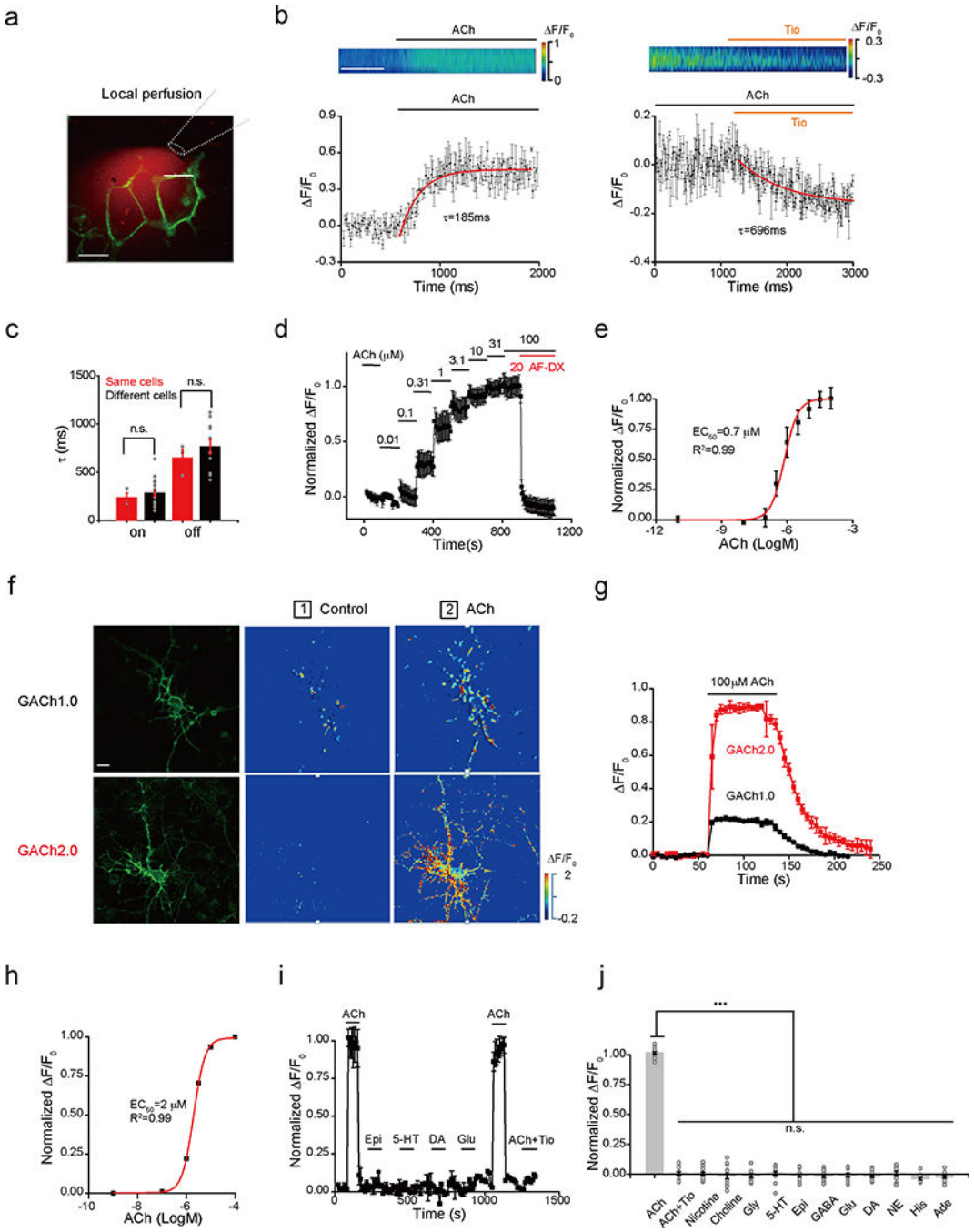

Figure 2. Characterization of GACh sensors in cultured HEK293T cells and neurons.

(**a**) Illustration of a fast perfusion system with a glass pipette filled with ACh and red Rhodamine-6G dye placed close to a GACh2.0 expressing cell. A white dash line indicates where the line scanning was performed.

(**b**) Upper, scanning traces of fluorescence responses of GACh2.0 expressing cells to application of ACh and Tio. Lower, plot shows fluorescence values of on and off responses of a GACh2.0 expressing cell to the application of ACh or Tio, averaged from 3 different

Author Manuscript Author Manuscript Author Manuscript Author Manuscript

ROIs on the scanning line. The original data was processed with 16× binning and plotted. The white line indicates 0.5 s.

(**c**) Averaged on and off time constants measured from the same (On: 233 ± 48 ms, $n = 3$ cells from 3 cultures; Off: 645 ± 90 ms, $n = 3$ cells from 3 cultures) and different (On: 279 ± 32 ms, $n = 18$ cells from 18 cultures; Off: 762 ± 75 ms, $n = 11$ cells from 11 cultures) cells. Note no statistic difference between the results obtained from the same and different cells ($p = 0.80$ for on kinetics, $p = 0.64$ for off kinetics).

(**d**) Averaged responses (3 trials from the same cell) of a GACh2.0 expressing HEK293T cell to ACh application. Note blockade of the responses by muscarinic antagonist AF-DX 384.

(**e**) Dose-dependent response plot of GACh2.0 expressing HEK293T cells to ACh application yielded $pEC_{50} = -6.12 \pm 0.11$ M, or $EC_{50} = 0.78 \pm 0.25$ μM, $n = 4$ cells from 4 cultures.

(**f**) Confocal GFP fluorescent and pseudocolor images of GACh1.0 and GACh2.0 expressing cultured cortical neurons in the normal bath solution and solution containing 100 μM ACh.

(**g**) Time course of the fluorescence response of GACh1.0 and GACh2.0 expressing cultured neurons (averaged from 3 independent trials of single neurons).

(**h**) Dose-dependent responses of GACh2.0 expressing cultured neurons ($pEC_{50} = -5.70 \pm 0.01$ M or $EC_{50} = 1.99 \pm 0.05$ μM; $n = 15$ neurons from 15 cultures).

(**i**) Responses of GACh2.0 expressing neurons to application of ACh and ACh-related compounds and other major neurotransmitters/modulators (averaged from 3 neurons in the same culture).

(**j**) Values for normalized $\Delta F/F_0$ of GACh2.0 expressing cells to application of 100 μM ACh with 2 μM tiotropium (Tio), 50 μM Nicotine, 100 μM Choline, 10 μM Glycine (Gly), 1 μM 5-HT, 10 μM Epinephrine (Epi), 10 μM GABA, 10 μM Glutamate (Glu), 20 μM Dopamine (DA), 200 μM Norepinephrine (NE), 1000 μM Histamine (His), 1 μM Adenosine (Ade) compared to application of ACh alone (ACh: 100.65 ± 7.61%, $n = 14$ ROIs with >10 cells each ROI; ACh+Tio: 0.19 ± 1.53%, $n = 14$ ROIs, $U = 196$, $p = 7.47E\text{-}6$; Nicotine: 0.32 ± 1.47%, $n = 15$ ROIs, $U = 210$, $p = 5.10E\text{-}6$; Choline: −1.46 ± 2.31%, $n = 15$ ROIs, $U = 210$, $p = 5.10E\text{-}6$; Glycine: −1.36 ± 1.58%, $n = 13$ ROIs, $U = 182$, $p = 1.13E\text{-}5$; 5-HT: 0.96 ± 1.11%, $n = 15$ ROIs, $U = 210$, $p = 5.10E\text{-}6$; Epi: −0.77 ± 1.35%, $n = 14$ ROIs, $U = 196$, $p = 7.47E\text{-}6$; GABA: −2.01 ± 1.11%, $n = 15$ ROIs, $U = 210$, $p = 5.10E\text{-}6$; Glu: −0.49 ± 1.45%, $n = 16$ ROIs, $U = 224$, $p = 3.57E\text{-}6$; DA: −0.83 ± 1.20%, $n = 15$ ROIs, $U = 210$, $p = 5.10E\text{-}6$; NE: −0.42 ± 1.63%, $n = 12$ ROIs, $U = 168$, $p = 1.75E\text{-}5$; His: −4.54 ± 0.66%, $n = 11$ ROIs, $U = 154$, $p = 2.81E\text{-}5$; Ade: −2.23 ± 1.05%, $n = 16$ ROIs, $U = 224$, $p = 3.57E\text{-}6$.

Data are shown with mean ± s.e.m, with error bars indicating s.e.m.

*, $p < 0.05$; **, $p < 0.01$; ***, $p < 0.001$; n.s., not significant (Mann-Whitney Rank Sum non-parametric tests, two-sides). All scale bars, 10 μm.

Author Manuscript
Author Manuscript
Author Manuscript
Author Manuscript

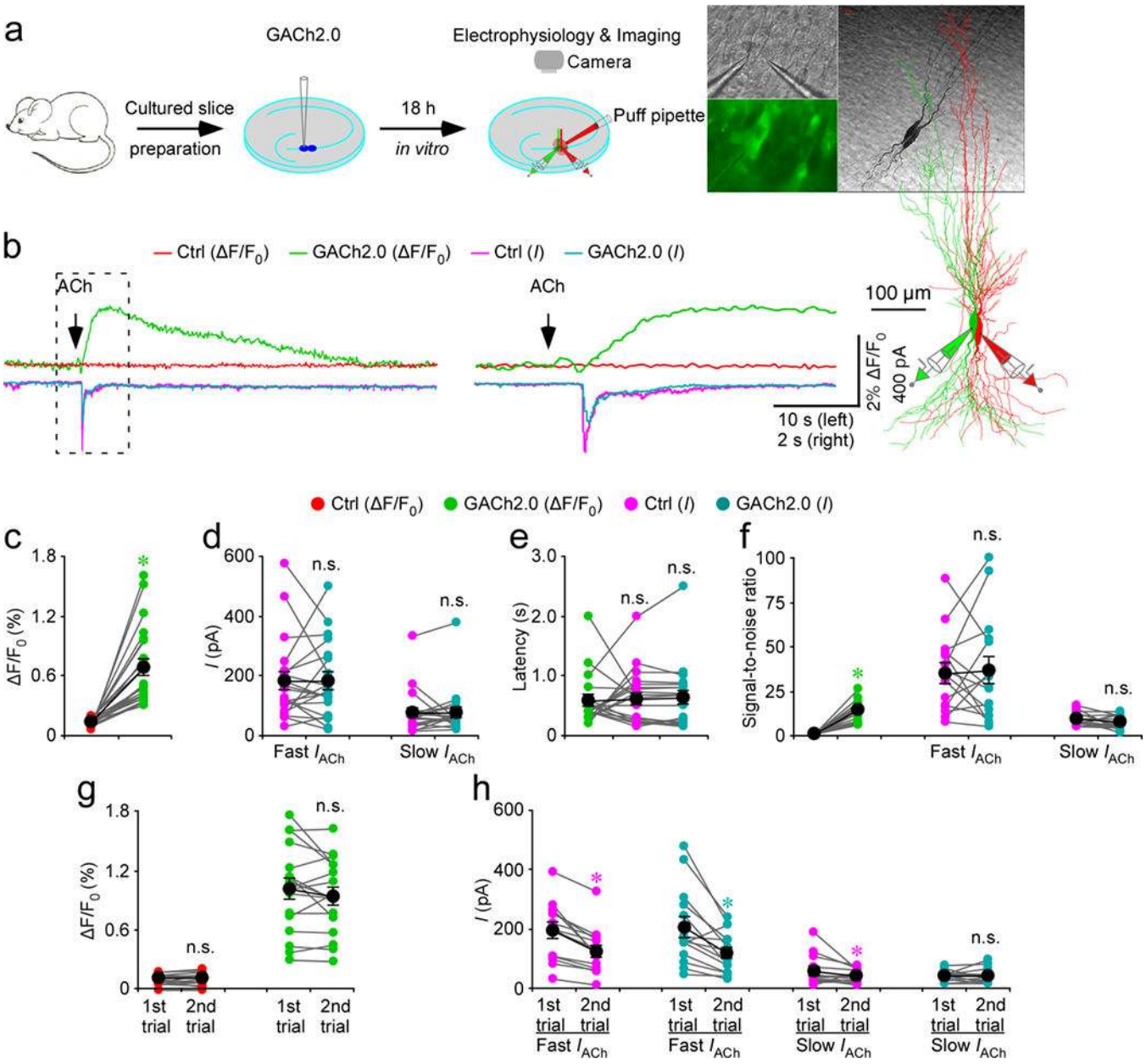

Figure 3. GACh2.0 detects rapid ACh application in brain slices.

(**a**) Schematic drawing outlines the design of simultaneous imaging and electrophysiological recording experiments in mouse cultured hippocampal slice preparation. Left insets show transmitted light (top), fluorescence microscopic (bottom) images of a pair of simultaneously recorded GACh2.0 expressing and neighboring control non-expressing CA3 neurons. Right insets show the biocytin-filled and reconstructed GACh2.0 expressing and non-expressing CA3 neurons.

(**b**) Left, simultaneous fluorescence and current responses of the pair of GACh2.0 expressing and neighboring control non-expressing CA3 neurons to a brief puff (500 ms) application of 100 mM acetylcholine (**ACh**). Right, the responses in the left rectangle box are shown again in an expanded time scale.

Author Manuscript Author Manuscript Author Manuscript Author Manuscript

(**c**) Values for the cholinergic fluorescence responses of GACh2.0 expressing CA3 neurons compared to non-expressing neurons (GACh2.0: 0.68 ± 0.08%; Ctrl: 0.14 ± 0.01%; Z = 4.015; p = 0.0005; n = 21 neurons from 9 animals).
(**d**) Values for the amplitudes of fast cholinergic current responses (GACh2.0: 180.9 ± 30.8 pA; Ctrl: 181.2 ± 28.4 pA; Z = −0.037; p = 0.97; n = 21 from 9 animals) and slow cholinergic current responses (GACh2.0: 76.2 ± 15.9 pA; Ctrl: 76.8 ± 17.0 pA; Z = 0.896; p = 0.37; n = 21 neurons from 9 animals) in GACh2.0 expressing CA3 neurons compared to non-expressing neurons.
(**e**) Values for the latencies of cholinergic current responses in non-expressing CA3 neurons (Ctrl: 611 ± 10 ms; Z = 0.523; p = 0.60) and GACh2.0 expressing (GACh2.0: 622 ± 12 ms; Z = 0.485; p = 0.62) compared to those of fluorescence responses of GACh2.0 expressing neurons (GACh2.0: 580 ± 9 ms; n = 21 neurons from 9 animals).
(**f**) Values for the signal-to-noise ratio (**SNR**) of cholinergic fluorescence responses of GACh2.0 expressing CA3 neurons compared to non-expressing neurons (GACh2.0: 14.0 ± 1.5; Ctrl: 1.0 ± 0.1; Z = 3.408; p = 0.001; n = 15 neurons from 6 animals), and that of fast (GACh2.0: 36.2 ± 7.7; Ctrl: 34.6 ± 5.7; Z = 0.170; p = 0.86; n = 15 neurons from 6 animals) and slow (GACh2.0: 7.5 ± 1.0; Ctrl: 9.0 ± 1.0; Z = −0.852; p = 0.39; n = 15 neurons from 6 animals) cholinergic current responses of GACh2.0 expressing CA3 neurons compared to non-expressing neurons. Note that SNR of cholinergic fluorescence responses of GACh2.0 expressing CA3 neurons is smaller than fast (GACh2.0: Z = 2.242; p = 0.015; Ctrl: Z = 3.124; p = 0.002), but larger than slow (GACh2.0: Z = −2.840; p = 0.005; Ctrl: Z = −2.669; p = 0.008) cholinergic current responses of GACh2.0 expressing CA3 neurons compared to non-expressing neurons.
(**g**) Values for the two fluorescence responses of non-expressing (1st: 0.11 ± 0.01%; 2nd: 0.11 ± 0.01%; Z = −0.142; p = 0.89; n = 17 neurons from 9 animals) and GACh2.0 expressing (1st: 1.01 ± 0.11%; 2nd: 0.94 ± 0.09%; Z = −1.138; p = 0.26; n = 17 neurons from 9 animals) CA3 neurons.
(h) Values for the two fast cholinergic current responses in non-expressing (1st: 190.9 ± 26.1 pA; 2nd: 124.1 ± 20.4 pA; Z = −3.296; p = 0.001; n = 17 neurons from 9 animals) and GACh2.0 expressing (1st: 203.8 ± 34.9 pA; 2nd: 119.3 ± 18.6 pA; Z = −2.856; p = 0.004; n = 17 neurons from 9 animals) CA3 neurons, and values for the two slow cholinergic current responses of non-expressing (1st: 56.4 ± 13.4 pA; 2nd: 39.0 ± 5.7 pA; Z = −2.166; p = 0.003; n = 17 neurons from 9 animals) and GACh2.0 expressing (1st: 41.6 ± 4.5 pA; 2nd: 41.7 ± 6.8 pA; Z = 0.940; p = 0.93; n = 17 neurons from 9 animals) CA3 neurons.
Data are shown with mean ± s.e.m, where large black dots indicate mean response, error bars indicate s.e.m. *, $p < 0.05$ (Wilcoxon tests, two-sides).

Author Manuscript Author Manuscript Author Manuscript Author Manuscript

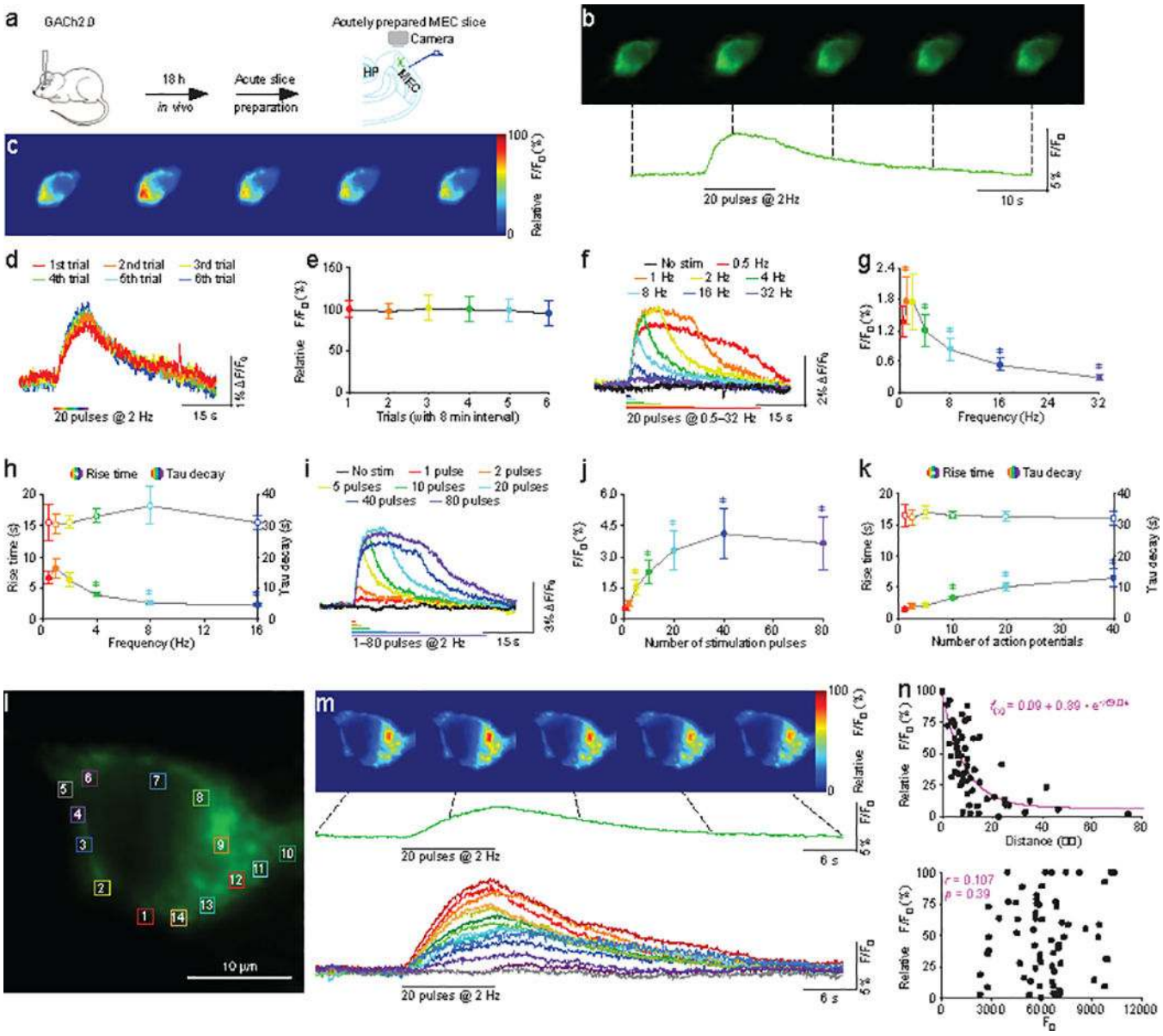

Figure 4. GACh2.0 reveals firing pattern-dependent restricted volume transmission in MEC.

(**a**) Schematic drawing outlines the design of stimulation-imaging experiments in mouse MEC preparation.

(**b**) Snapshots of fluorescence responses of a GACh2.0 expressing stellate cell to local electrical stimuli.

(**c**) Relative fluorescence responses of the GACh2.0 expressing stellate cell to local electrical stimuli shown in a heat map format.

(**d**) Fluorescence responses of a GACh2.0 expressing MEC stellate neuron to repetitive layer 1 electrical stimulation every 8 minutes.

(**e**) Values for the subsequent fluorescence responses of GACh2.0 MEC stellate neurons to the multiple layer 1 electrical stimulation at time interval of 8 min (2nd: 1.58 ± 0.15%, $Z = -0.534$; $p = 0.59$; 3rd: 1.65 ± 0.25%, $Z = -0.178$; $p = 0.86$; 4th: 1.62 ± 0.25%, $Z = 0.222$; p

Author Manuscript Author Manuscript Author Manuscript Author Manuscript

= 0.82; 5th: 1.61 ± 0.22%, $Z = 0.051$; $p = 0.96$; 6th: 1.55 ± 0.23%, $Z = -0.800$; $p = 0.42$; $n =$ 11 neurons from 7 animals) compared to the first fluorescence response (1st: 1.63 ± 0.16%).

(**f**) Fluorescence responses of a GACh2.0 expressing MEC stellate neuron to electrical stimuli consisting of a train of 20 pulses at varied frequency.

(**g**) Values for the peak fluorescence responses of GACh2.0 expressing MEC stellate neurons to electrical stimulations consisting of a train of 20 pulses at higher frequency (1 Hz: 1.75 ± 0.47%, $Z = 2.606$; $p = 0.009$; 2 Hz: 1.74 ± 0.53%, $Z = 1.726$; $p = 0.08$; 4 Hz: 1.19 ± 0.44%, $Z = -1.746$; $p = 0.140$; 8 Hz: 0.82 ± 0.22%, $Z = -3.107$; $p = 0.002$; 16 Hz: 0.53 ± 0.12%, $Z = -3.296$; $p = 0.001$; 32 Hz: 0.29 ± 0.06%, $Z = -3.296$; $p = 0.001$; $n = 14$ neurons from 9 animals) compared to the lowest frequency tested (0.5 Hz: 1.34 ± 0.30%).

(**h**) Values for 10–90% rise time of the fluorescence responses of GACh2.0 expressing MEC stellate neurons to electrical stimulations consisting of a train of 20 pulses at higher frequency (1 Hz: 8.1 ± 1.5 s, $Z = 1.859$; $p = 0.06$; 2 Hz: 6.2 ± 1.1 s, $Z = 0.001$; $p = 0.99$; 4 Hz: 3.8 ± 0.3 s; $Z = -2.197$; $p =$0.028; 8 Hz: 2.4 ± 0.3 s, $Z = -2.366$; $p = 0.018$; 16 Hz: 2.1 ± 0.3 s, $Z = -2.366$; $p = 0.018$; $n = 7$ neurons from 5 animals) compared to the lowest frequency tested (0.5 Hz: 6.5 ± 0.9 s), and values for decay time constant of the fluorescence responses of GACh2.0 expressing MEC stellate neurons to electrical stimulations consisting of a train of 20 pulses at higher frequency (1 Hz: 30.4 ± 3.1 s, $Z = 0.169$; $p = 0.87$; 2 Hz: 30.8 ± 2.0 s, $Z = 0.338$; $p = 0.74$; 4 Hz: 33.0 ± 2.1 s; $Z = 0.338$; $p = 0.74$; 8 Hz: 36.4 ± 6.1 s, $Z = 1.363$; $p = 0.17$; 16 Hz: 31.0 ± 2.4 s, $Z = 0.169$; $p = 0.87$; $n = 7$ neurons from 5 animals) compared to the lowest frequency tested (0.5 Hz: 30.8 ± 5.7 s).

(**i**) Fluorescence responses of GACh2.0 expressing MEC stellate neuron to electrical stimulations consisting of a train of up to 80 pulses at 2 Hz.

(**j**) Values for the maximal responses of GACh2.0 expressing MEC stellate neurons to electrical stimulations consisting of a train of up to 80 pulses at 2 Hz (2 pulses: 0.70 ± 0.15%, $Z = 1.960$; $p = 0.05$; 5 pulses: 1.53 ± 0.38%, $Z = 2.521$; $p = 0.012$; 10 pulses: 2.22 ± 0.56%, $Z = 2.521$; $p = 0.012$; 20 pulses: 3.29 ± 0.95%, $Z = 2.521$; $p = 0.012$; 40 pulses: 4.07 ± 1.22%, $Z = 2.366$; $p = 0.017$; 80 pulse: 3.65 ± 1.30%, $Z = 2.366$; $p = 0.017$; $n = 8$ neurons from 4 animals) compared to single pulses (1 pulse: 0.50 ± 0.09%).

(**k**) Values for 10–90% rise time of the maximal responses of GACh2.0 expressing MEC stellate neurons to electrical stimulations consisting of a train of up to 80 pulses at 2 Hz (2 pulses: 1.8 ± 0.4 s, $Z = 1.718$; $p = 0.08$; 5 pulses: 2.0 ± 0.3 s, $Z = 1.955$; $p = 0.05$; 10 pulses: 3.3 ± 0.3 s, $Z = 2.666$; $p = 0.008$; 20 pulses: 5.0 ± 0.6 s, $Z = 2.666$; $p = 0.008$; 40 pulses: 6.5 ± 1.4 s, $Z = 2.666$; $p = 0.008$; $n = 9$ neurons from 6 animals) compared to single pulses (1 pulse: 1.3 ± 0.3 s), and decay time constant of the maximal responses of GACh2.0 expressing MEC stellate neurons to electrical stimulations consisting of a train of up to 80 pulses at 2 Hz (2 pulses: 32.2 ± 2.6 s, $Z = -0.296$; $p = 0.77$; 5 pulses: 33.9 ± 2.1 s, $Z =$ 0.178; $p = 0.86$; 10 pulses: 32.8 ± 1.1 s, $Z = -0.415$; $p = 0.68$; 20 pulses: 32.7 ± 1.7 s, $Z =$ −0.338; $p = 0.75$; 40 pulses: 31.8 ± 2.3 s, $Z = -0.415$; $p = 0.68$; $n = 9$ neurons from 6 animals) compared to single pulses (1 pulse: 32.9 ± 3.5 s). Note the stimulation pulse number-dependent increase in 10–90% rise time, but not in decay time constant.

(**l**) A snapshot of another GACh2.0 expressing stellate cell.

(**m**) Upper, snapshots of fluorescence responses of the GACh2.0 expressing neuron in (**l**) to a minimal L1 electrical stimulation. The fluorescence recording trace immediately below shows the average fluorescence response of the neuron. The lower fluorescence recording

Author Manuscript Author Manuscript Author Manuscript Author Manuscript

traces show $\Delta F/F_0$ responses in the subcellular regions of interest (ROIs) marked by color squares (~1.5 μm x ~1.5 μm) in (**l**). Note the largest $\Delta F/F_0$ responses seen in two red ROIs (#9 and #1) suggestive of possible activation of multiple cholinergic fibers and/or release sites, and the slower rising times of smaller responses in other ROIs expected for diffused ACh.

(**n**) Upper, plot of $\Delta F/F_0$ responses in ROIs against the distance from the ROI with maximal $\Delta F/F_0$. The data points ($n = 67$ from 6 neurons of 6 animals) were arbitrarily fitted to a single exponential decay function (pink line), resulting in an estimated volume spread length constant of ~9 μm. Lower, plot of $\Delta F/F_0$ against F_0 indicates no correlation between $\Delta F/F_0$ and F_0 ($n = 67$; two-sides Normality test $p = 0.06$; two-sides Constant variance test $p = 0.80$; $r = 0.107$; $p = 0.39$; two-sides Linear regression t test). The relative $\Delta F/F_0$ responses, or the $\Delta F/F_0$ responses normalized to the largest $\Delta F/F_0$ responses in the same neurons, were used in analysis in (**n**).

Data are shown with mean ± s.e.m, where large black dots indicate mean response, error bars indicate s.e.m. Experiments in (**b**),(**d**),(**f**), (**i**),(**l**),(**m**) were repeated independently for more than 6 animals with similar results. *, $p < 0.05$ (Wilcoxon tests, two-sides).

Author Manuscript
Author Manuscript
Author Manuscript
Author Manuscript

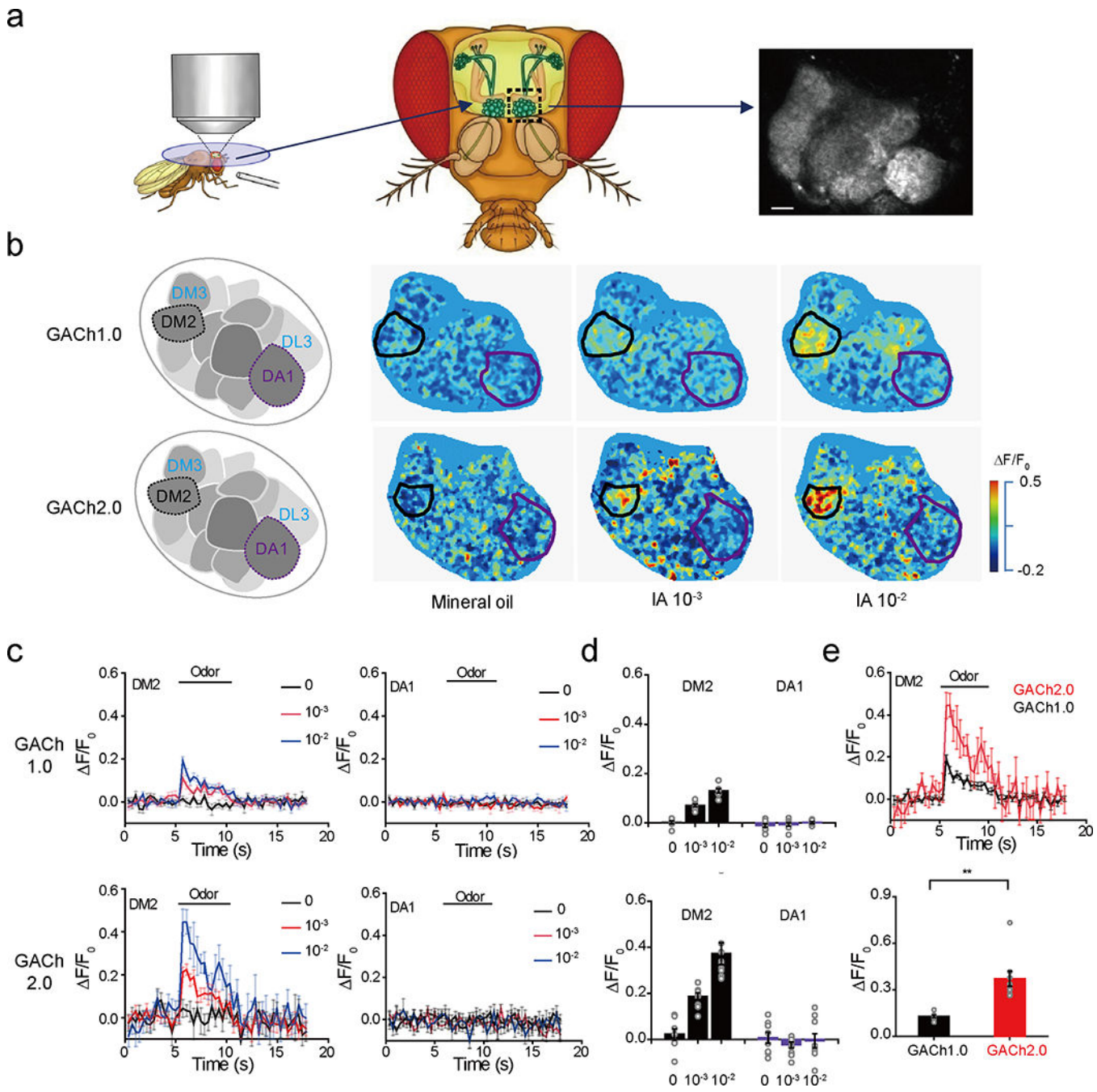

Figure 5. GACh sensors reveal dynamics of endogenous ACh release in *Drosophila*.

(**a**) Schematic illustration of the two-photon imaging setup of the *Drosophila* olfactory system. Odor was delivered near the antenna (Left) and GACh signals were measured in the antennal lobe area of GH146-Gal4: UAS-GACh flies (Right).

(**b**) Pseudocolor images of GACh expressing antenna lobes show fluorescence responses to mineral oil and odor isoamyl acetate (IA).

Author Manuscript Author Manuscript Author Manuscript Author Manuscript

(**c**) Time courses of the IA-dependent responses in DM2 and DA1 glomeruli of GACh1.0 (upper plots) and GACh2.0 (lower plots) expressing antenna lobes. The traces were averaged from 3 trials in the same fly.

(**d**) Values for the maximal $\Delta F/F_0$ in DM2 and DA1 glomeruli of GACh1.0 (upper plot; DM2: 0.29 ± 0.49%, $n = 9$ flies; DA1: −1.01 ± 0.68%, $n = 9$ flies, $U = 55$, $p = 0.22$ for mineral oil; DM2: 7.02 ± 0.56%, $n = 9$ flies; DA1: −0.61 ± 0.80%, $n = 9$ flies, $U = 81$, $p =$ 4.12E-4 for 10–3 IA; DM2: 12.97 ± 1.28%, $n = 7$ flies; DA1: 0.17 ± 0.39%, $n = 7$ flies, $U =$ 49, $p = 0.002$ for IA 10–2) and GACh2.0 (lower plot; DM2: 2.27 ± 2.34%, $n = 8$ flies; DA1: −0.73 ± 1.41%, $n = 8$ flies, $U = 35$, $p = 0.80$ for mineral oil, DM2: 18.78 ± 1.36%, $n = 10$ flies; DA1: −2.37 ± 1.06%, $n = 10$ flies, $U = 100$, $p =$ 1.83E-4 for 10–3 IA; DM2: 37.30 ± 4.79%, $n = 9$ flies; DA1: −0.55 ± 2.68%, $n = 9$ flies, $U = 81$, $p =$ 4.12E-4 for 10–2 IA) expressing antenna lobes.

(**e**) Upper, IA-evoked responses in DM2 glomerulus of GACh1.0 and GACh2.0 transgenic flies. Lower: values for the maximal $\Delta F/F_0$ in DM2 glomerulus of GACh1.0 and GACh2.0 transgenic flies (GACh1.0: 12.97 ± 1.28%, $n = 7$ flies; GACh2.0: 37.30 ± 4.79% $n = 9$ flies; $U = 63$, $p = 0.001$).

Data are shown with mean ± s.e.m, with error bars indicate s.e.m. Experiments in (**b**) were repeated independently for more than 7 flies with similar results. **, $p < 0.01$ (Mann-Whitney Rank Sum non-parametric tests, two-sides). All scale bars, 10 μm.

Author Manuscript Author Manuscript Author Manuscript Author Manuscript

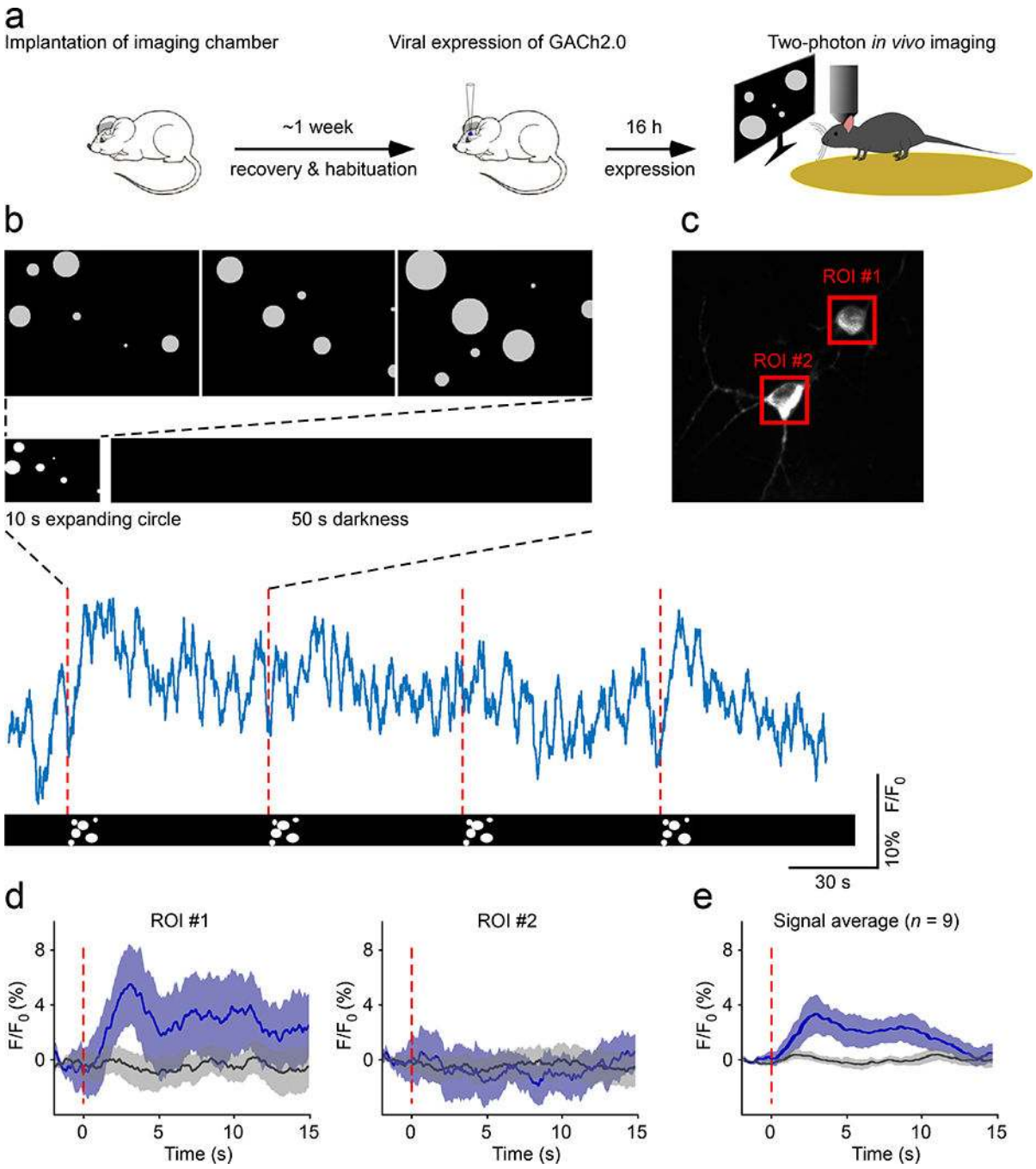

Figure 6. Attention-engaging visual stimuli evoke ACh release in behaving mice.

(**a**) Schematic drawing outlines the design of *in vivo* imaging experiments.

(**b**) Upper, schematic representation of the visual stimulus applied to head-fixed behaving mice. The visual stimulus consists of 10 seconds of expanding white circles appearing at random locations on the screen, followed by 50 seconds of darkness. Lower, 4-minute fluorescence response traces corresponding to the four repetitions of single stimuli.

(**c**) An imaged region (100 × 100 μm, 120 μm deep) contains two GACh2.0 expressing neurons with the red squares indicating regions of interest (ROIs).

Author Manuscript Author Manuscript Author Manuscript Author Manuscript

(**d**) Mean fluorescence responses from ROIs shown in (**b**). The fluorescence response traces were divided into 10 second segments with every minute containing one 10-s trace corresponding to the period of visual stimulus and five 10-s traces corresponding to periods of darkness. The signal from the middle three dark segments (black line) was compared to the signal from the visual stimulus segments (blue line; 15 trials per region). Shaded bands around the solid blue trace show the 95% confidence interval obtained by bootstrap. Note that ROI #1, but not ROI #2, shows an increase in fluorescence responses to the visual stimulus.

(**e**) Average fluorescence responses obtained during the period of visual stimulation compared to those during the period of darkness (Visual: 3.37 ± 2.26%; Dark: 0.05 ± 0.83%; $Z = -2.666$, $p = 0.008$; $n = 9$ neurons from 8 animals). Note the same ACh signals observed after 1-day ($n = 5$ neurons from 4 animals), 2-day ($n = 2$ neurons from 2 animals), and 4–6-day ($n = 2$ neurons from 2 animals) *in vivo* Sindbis or rapid AAV viral expression, which suggest the suitability of GACh sensors for multiple-day imaging, and the analysis made from the pooled data.

Data are shown with mean ± s.e.m, with shaded bands indicate s.e.m. Wilcoxon tests performed in (**e**), two-sides.